UNITED NATIONS EDUCATIONAL, SCIENTIFIC AND CULTURAL ORGANIZATION
INTERNATIONAL ATOMIC ENERGY AGENCY
INTERNATIONAL CENTRE FOR THEORETICAL PHYSICS
I.C.T.P., P.O. BOX 586, 34100 TRIESTE, ITALY, CABLE: CENTRATOM TRIESTE

H4.SMR/984-5

Winter College on Quantum Optics: Novel Radiation Sources

3-21 March 1997

Wave packet dynamics
Quantum state preparation and measurements
Quantum effects in Paul traps

W. Schleich

Abteilung für Quantenphysik, Universität Ulm, Germany

~~Submitted to~~ J. Phys. A

Space-time structures in simple quantum systems

Frank Großmann[a], Jan-Michael Rost[a] and Wolfgang P. Schleich[b]

[a] *Albert-Ludwigs-Universität, Fakultät für Physik, Hermann-Herder-Str. 3, D-79104 Freiburg, Germany*

[b] *Abteilung für Quantenphysik, Universität Ulm D-89069 Ulm, Germany*

Abstract

Recently W. Kinzel [Phys. Bl. **51**, 1190 (1995)] has argued that even simple quantum systems can exhibit surprising phenomena. As an example he presented the formation of canals and ridges in the time dependent probability density of a particle caught in a square well with infinitely high walls. We show how these structures emerge from the wavefunction and present a simple derivation of their location in the space-time continuum.

Prominent structures in the probability density of quantum states have attracted much attention. They are known as *scars* for time independent problems where certain eigenstates have regions of high amplitude along periodic orbits of the classical dynamics for the same system [1]. This phenomenon has helped to understand the links between classical and quantum mechanics in more detail [2]. In the time domain the reconstruction or partial reconstruction of the initial spatial probability distribution is known as *revivals* and has played an important role in the understanding of wavepacket dynamics [3]. The combination of spatial and temporal structures in a probability density has only recently entered the focus of attention. Kinzel [4] has studied numerically the time-evolution of a particle in an infinitely high potential well. He used a Gaussian initial wavepacket centered close to the left wall and furnished with a momentum pointing towards the right. In a three dimensional plot of the absolute square of the wavefunction over position and time, regular structures in the shape of valleys and hills appear. Clearly, such structures must be an interference phenomenon. However, their origin is not as obvious as one might expect for such a simple system and has not been given in [4]. Berry and Klein have found similar patterns in the Talbot effect and Berry has also studied fractal probability densities in the space-time continuum for multi-dimensional box potentials [5]. In the latter case he has used a special initial state with equal probability amplitude at each point in the box. Stifter et al. [6], using Gaussian initial wavefunctions, have shown that the structures in the probability distribution can be viewed as a consequence of the interference term in the Wigner function. In this letter we will use an initial state which is composed of the first N eigenfunctions with equal weights. This allows us to study the emerging pattern in space-time as a function of N. It will turn out that the structures in the amplitude distribution arise from a cancellation of terms in the wavefunction and that the parameter N controls the resolution of the pattern. Our analysis borrows a mathematical technique which is familiar in the context of Jacobi's theta functions. We will also discuss briefly possible generalizations of the phenomenon to other systems.

Any initial wavefunction $\Psi_0(x)$ in the box extending from $x = 0$ to $x = L$ may be

expanded in the basis of eigenfunctions

$$\phi_n(x) = \sqrt{\frac{2}{L}} \sin\left(\frac{n\pi}{L}x\right) \tag{1}$$

with coefficients

$$a_n = \int_0^L dx \phi_n(x) \Psi_0(x). \tag{2}$$

The corresponding eigenenergies

$$E_n = n^2 \frac{1}{2m}\left(\frac{\hbar\pi}{L}\right)^2 = n^2 \hbar \frac{2\pi}{T}, \tag{3}$$

with $n = 1, 2, 3, \ldots$ determine the so-called revival time $T = 4mL^2/(\pi\hbar)$ of the wavepacket in the box [7].

To keep the argument transparent we now discuss an initial wavefunction Ψ_0 consisting of N equally contributing eigenfunctions, i.e. $a_n = 1$, for $n = 1, \ldots, N$ and $a_n = 0$ for $n > N$. In dimensionless variables $\xi \equiv x/L$ and $\tau \equiv t/T$ for position and time the normalized wavefunction reads

$$\Psi(\xi, \tau) = \sqrt{\frac{2}{N}} \sum_{n=1}^{N} \sin(n\pi\xi) \exp(-2\pi i n^2 \tau). \tag{4}$$

Figure 1 displays the wavefunctions at $\tau = 0$ made up of 20, 50 and 100 eigenfunctions, respectively. We note that increasing N shifts the center of the initial state towards the left and leads to sharper localization in position. Figure 2 shows a density plot of the position and time dependent probability amplitude in the (ξ, τ) plane represented by the absolute value of a wavefunction consisting of 20 eigenfunctions. We observe characteristic rays where $|\Psi(\xi, \tau)|$ assumes low (darkness) and high (brightness) values. These rays emerge either from the left corner $(\xi = 0, \tau = 0)$ or from the right corner $(\xi = 1, \tau = 0)$ of the space-time strip. Moreover, there is a characteristic asymmetry between the two types of rays: Along the ones from the left corner the wavefunction shows low probability, that is canals. In contrast some of the rays originating from the right corner have high probability, that is ridges. However, canals constantly cut through these ridges creating a chopped structure as seen in the line

connecting the upper left corner with the lower right corner in Figure 2. We also recognize that additional rays enter the space-time strip from its sides.

An educated guess for the rays is

$$\xi = l + 2k\tau \tag{5}$$

where l and k are integers. Indeed for $l = 0$ and $k \geq 0$, Eq. (5) describes the rays emerging from the left corner, whereas for $l = 1$ and $k \leq 0$ we find the rays whose origin is the right corner. The other values of l such as $l < 0$ and $k > 0$ or $l > 1$ and $k < 0$ give the rays entering the strip at nonzero values of τ.

We gain deeper insight into the functional form Eq. (5) of these rays when we recall that according to M. Born [8] the time evolution of a particle with wavefunction Ψ_0 in the box is identical to that of a free particle prepared initially in a periodic array

$$\Psi_p(\xi, \tau = 0) = \sum_{m=-\infty}^{\infty} \Psi_0^-(\xi + 2m) \tag{6}$$

of antisymmetric wavefunctions

$$\Psi_0^-(\xi) \equiv \Psi_0(\xi) - \Psi_0(-\xi). \tag{7}$$

The period of this array is twice the length of the box. Hence in Eq. (5) even values of $l = 2m$ correspond to the positions of the left wall and its mirror images. In contrast odd values $l = 2m + 1$ represent the positions of the right wall and its mirror images. Therefore the rays Eq. (5) are the space-time trajectories of a free particle starting at time $\tau = 0$ at the right or left wall and their mirror images. Note that according to Eq. (5) the particle propagates with the dimensionless velocity $v_k \equiv \frac{d\xi}{d\tau} = 2k$. Since k is integer v_k assumes only discrete values. This quantization of velocity is a consequence of the periodicity of the array.

We emphasize that this discussion of the free propagation of the array also throws some light on the difference in behavior of $\Psi(\xi, \tau)$ along the rays emerging from the two corners $(\xi = 2m, \tau = 0)$ and $(\xi = 2m + 1, \tau = 0)$ corresponding either to the left or the right wall of the box and their mirror images. Indeed these walls are different: Whereas the left wall

marks the beginning of the periodicity interval of period 2 the right wall is inserted at $\xi = 1$ as to retain from all periodic functions the antisymmetric ones, only. This procedure is necessary since only the latter vanish at the walls at $\xi = 0$ and $\xi = 1$ and hence satisfy the required boundary conditions.

In order to fathom the mathematical reason for the suppression of the wavefunction along some of the rays, Eq. (5), in the (ξ, τ) plane, we now write the sine function in the wavefunction, Eq. (4), in terms of exponentials,

$$\Psi(\xi, \tau) = \sqrt{\frac{2}{N}} \frac{1}{2i} \left\{ \vartheta(\xi, \tau) - \vartheta(-\xi, \tau) \right\}, \tag{8}$$

where we have introduced the finite theta sum

$$\vartheta(\xi, \tau) \equiv \sum_{n=1}^{N} q^{n^2} e^{in\pi\xi}, \tag{9}$$

with $q \equiv \exp(-2\pi i \tau)$ [9]. The behavior of the wavefunction along the rays $\xi = l + 2k\tau$ follows from

$$\vartheta[\xi \doteq \pm(l + 2k\tau), \tau] = \sum_{n=1}^{N} (-1)^{nl} \exp\left\{ -2\pi i \tau (n^2 \mp nk) \right\}. \tag{10}$$

When we complete the square in the exponent we find

$$\vartheta[\xi = \pm(l + 2k\tau), \tau] = q^{-(k/2)^2} \sum_{n=1}^{N} (-1)^{nl} q^{(n \mp k/2)^2} \tag{11}$$

and hence the wavefunction along the rays Eq. (5) reads

$$\Psi(\xi = l + 2k\tau, \tau) = \sqrt{\frac{2}{N}} \frac{1}{2i} q^{-(k/2)^2} \sum_{n=1}^{N} (-1)^{nl} \left[q^{(n-k/2)^2} - q^{(n+k/2)^2} \right]. \tag{12}$$

We note that each term contributing to this sum is the difference of the two terms $q^{(n-k/2)^2}$ and $q^{(n+k/2)^2}$. Since the powers $(n - k/2)^2$ and $(n + k/2)^2$ are shifted by the number k determining the steepness of the ray, we expect a partial cancellation of these terms provided the number N of terms is much larger than k. Here the prefactor $(-1)^{nl}$ plays a crucial role. Indeed when l is even this factor is unity and cancellation takes place. However, when l is odd the situation is more complicated. Now cancellation only occurs when k is even. Before we show this we note from Eq. (12) the symmetry relation

$$\Psi(\xi = l - 2k\tau, \tau) = -\Psi(\xi = l + 2k\tau, \tau) \tag{13}$$

which allows us to confine our discussion to positive values of k only.

We start our analysis of this cancellation effect in Eq. (12) by introducing the summation index $j \equiv n - k$ in the summation of the first term which yields

$$\Psi(\xi = l + 2k\tau, \tau) = \sqrt{\frac{2}{N}}\frac{1}{2i}q^{-(k/2)^2}\Big\{(-1)^{kl}\sum_{j=1-k}^{N-k}(-1)^{jl}q^{(j+k/2)^2} - \sum_{n=1}^{N}(-1)^{nl}q^{(n+k/2)^2}\Big\}. \tag{14}$$

When we recall the relations

$$\sum_{j=1-k}^{N-k} d_j = \sum_{j=1-k}^{0} d_j + \sum_{j=1}^{N-k} d_j = \sum_{n=1}^{k} d_{n-k} + \sum_{j=1}^{N-k} d_j \tag{15}$$

and

$$\sum_{n=1}^{N} d_n = \sum_{n=1}^{N-k} d_n + \sum_{n=N-k+1}^{N} d_n = \sum_{n=1}^{N-k} d_n + \sum_{j=1}^{k} d_{j-k+N} \tag{16}$$

valid for arbitrary coefficients d_j the wavefunction Ψ along the rays $\xi = l + 2k\tau$ takes the form

$$\begin{aligned}\Psi(\xi = l + 2k\tau, \tau) = \sqrt{\frac{2}{N}}\frac{1}{2i}q^{-(k/2)^2}\Big\{\Big[(-1)^{kl} - 1\Big]S_{k,l}(N, \tau) \\ + \sum_{n=1}^{k}(-1)^{nl}\Big[q^{(n-k/2)^2} - (-1)^{(N-k)l}q^{(n-k/2+N)^2}\Big]\Big\}.\end{aligned} \tag{17}$$

where

$$S_{k,l}(N, \tau) = \sum_{j=1}^{N-k}(-1)^{jl}\exp[-2\pi i(j + k/2)^2\tau]. \tag{18}$$

From Eq. (17) we recognize that for even values of l or k the prefactor of the first sum $S_{k,l}$ vanishes. Moreover, each term of the remaining sum is of the order of unity since $|q| = |\exp(-2\pi i\tau)| = 1$. Hence we can estimate this sum consisting of k differences of order 2 by $2|k|$. This provides us with the upper bound

$$|\Psi(\xi = 2m + 2k\tau, \tau)| \leq \sqrt{\frac{2}{N}}|k| \tag{19}$$

for the absolute value of the wave function along the rays $\xi = 2m + 2k\tau$ starting from the left wall and its mirror images. Similarly we find along the even rays $\xi = 2m + 1 + 4k\tau$ emerging from the right wall and its mirror images

$$|\Psi(\xi = 2m + 1 + 4k\tau, \tau)| \leq \sqrt{\frac{2}{N}}|2k|. \tag{20}$$

When we confine ourselves to rays of large slope that is small values of $|k|$, that is $|k| \ll N$, we find the inequalities

$$|\Psi(\xi = 2m + 2k\tau, \tau)| \ll 1 \tag{21}$$

and

$$|\Psi(\xi = 2m + 1 + 4k\tau, \tau)| \ll 1. \tag{22}$$

We recall that the modulus $|\Psi(\xi, \tau)|$ of any normalized wavefunction in the box of unit length is unity on average. Hence the inequalities Eqs. (21,22) predict that along these rays the modulus $|\Psi|$ falls far below the average value and canals form along these rays. We also note from Eqs. (19,20) that for increasing $|k|$, that is decreasing steepness of the rays the cancellation of terms in the sum Eq. (12) becomes less perfect and the canals become less pronounced in complete agreement with Figure 2.

Our treatment brings out most clearly that the formation of the canals is indeed a consequence of quantum interference in the wavefunction: The inequalities (21) and (22) follow from the cancellation in Eq. (17) which we can trace back to the fact that any wavefunction in the box is a superposition of a right and a left running wave. These waves have a fixed phase difference π, which translates itself into the difference of ϑ sums in Eq. (8). The difference reflects the fact that the energy eigenfunctions have to satisfy the boundary conditions at the walls. This picture is in complete agreement with Ref. [6] which used the Wigner representation to identify these canals as a consequence of the Wigner interference term between the two waves moving against each other.

Let us now briefly discuss the case of odd values of l *and* k when the prefactor of $S_{k,l}$ in Eq. (17) does not vanish. Hence when we now estimate $|\Psi|$ along these rays we have to take into account the sum $S_{k,l}$. In particular we have to study its dependence on time τ. Since the sum is similar to the one discussed in the context of curlicues [10] or fractional

revivals [5,11] we can simply borrow the results of these studies. We find [12] times τ, that is certain rational values of the revival time T for which partial cancellation in $S_{k,l}$ takes place. For these times the wave function Ψ falls, as in the case of the canals, far below its average value of unity. However, there also exist times τ where the individual terms in $S_{k,l}$ superpose constructively. In this case the sum $S_{k,l}$, and not the second sum in Eq. (17), is the dominant contribution to Ψ giving rise to distinct maxima along these rays. From Figure 2 we see that indeed every second ray propagating from $(\xi = 1, \tau = 0)$ to the left displays a complicated chopped structure, where for most of the ray, a ridge like behavior is seen. Again this phenomenon stands out most clearly for steep rays, i. e. small values of k.

Let us mention that this behavior depends sensitively on the total number of eigenfunctions N. The pattern becomes richer for larger values of N. This fact can be interpreted in the way that an initial state with a large number N of eigenstates resolves the features of the dynamics in the box to a much higher degree than for N small. Our derivation in terms of the eigenfunction expansion directly shows for all cases, l even or odd and k even or odd, that the number of rays $|k|$ which are visible depends on the number of eigenfunctions N contained in the wavefunction. Since the eigenfunctions of a box represent a Fourier basis. by Fourier analyzing wavepackets in other potentials one could make use of the methods given here.

We conclude by briefly discussing generalizations of these space-time structures. According to M. Born [8] and Eqs. (6,7) the boundary conditions of the box impose the antisymmetry of two waves moving against each other. Mimicing this symmetry in a molecular type of potential Stifter et al. [6] were able to produce similar effects. Moreover, in another formulation of the probability density in the energy representation Stifter at al. [13] have identified the characteristic space-time lines and have given a relativistic extension. We also recall that the quantum mechanical problem of a particle on a ring can be mapped onto the box problem, if the same boundary conditions are fulfilled. This can be achieved by subtracting opposite angular momentum eigenstates from each other. Let us finally mention that the corresponding problem in classical wave mechanics, i. e. a vibrating string clamped

at $\xi = 0$ and $\xi = 1$, shows a much simpler structure in the (ξ, τ) plane because its spectrum is linear in n.

In summary we have shown that the space-time structures in the quantum mechanical probability amplitude for a particle in a square well result from a cancellation in the eigenfunction expansion, Eq. (4). By using the wavefunction's Jacobi theta function-like properties represented in Eq. (11) we were able to explain the canals and also the chopped ridges along the rays, Eq. (5), in (ξ, τ) space. The details of these space-time patterns are indeed a property of the wavefunction itself. How much of these details is revealed depends sensitively on the initial wavefunction.

Financial support by the Deutsche Forschungsgemeinschaft through Sonderforschungsbereich 276 and the Gerhard-Hess-Programm, as well as valuable discussions with Gernot Alber, John Briggs, Jens Marklof, Peter Stifter and Alexander Kaplan are gratefully acknowledged.

REFERENCES

[1] Heller E J 1984 Phys. Rev. Lett. **53** 1515

[2] Heller E J and Tomsovic S July 1993 Physics Today pp 38

[3] Alber G and Zoller P 1991 Phys. Rep. **199** 231

[4] Kinzel W 1995 Phys. Bl. **51** 1190

[5] Berry M V and Klein S 1996 J. Mod. Optics **43** 2139; Berry M V 1996 J. Phys. A **29** 6617

[6] Stifter P Leichtle C Schleich W P Marklof J submitted to Phys Bl

[7] Stifter P Leichtle C Lamb W E and Schleich W P preprint

[8] Born M 1958 Z. Phys. **153** 372

[9] Note that the finite theta sum is closely related to the Jacobi theta functions discussed in: Whittaker E T and Watson G N 1980 *A Course of Modern Analysis* (Cambridge: Cambridge University Press) chapter XXI. Hence, we can carry over the methods used there to demonstrate the quasi periodicity of the theta functions to derive similar relations for ϑ. For a recent review of asymptotic properties of Jacobi theta functions. see also: Marklof J submitted to the proceedings of the IMA workshop *Emerging Applications of Number Theory: Quantum Mechanics*, Institute for Mathematics and its Applications, Minneapolis, July 1996

[10] Berry M V and Goldberg J 1988 Nonlinearity **1** 1

[11] Leichtle C Averbukh I Sh and Schleich W P 1996 Phys. Rev. Lett. **77** 3999

[12] This also follows from the original wavefunction expansion, Eq. (4)

[13] Stifter P Kaplan A Schleich W P preprint

FIGURES

Fig. 1: Initial wavefunctions $\Psi_0(\xi, \tau = 0)$ resulting from superpositions of $N = 20$ (solid line), $N = 50$ (long dash) and $N = 100$ (short dash) equally weighted eigenfunctions of the box potential. For increasing number N of contributing eigenstates the initial wavepacket gets narrower and its center approaches the left wall of the box.

Fig. 2: Density plot of the absolute value $|\Psi(\xi, \tau)|$ of a wavefunction in the (ξ, τ) space-time strip. Darkness displays a low and brightness a high functional value. We note that canals of different steepness emerge from the lower right or left corners of the strip. Moreover canals enter from the sides. For this example we have considered a wavefunction consisting of 20 eigenfunctions.

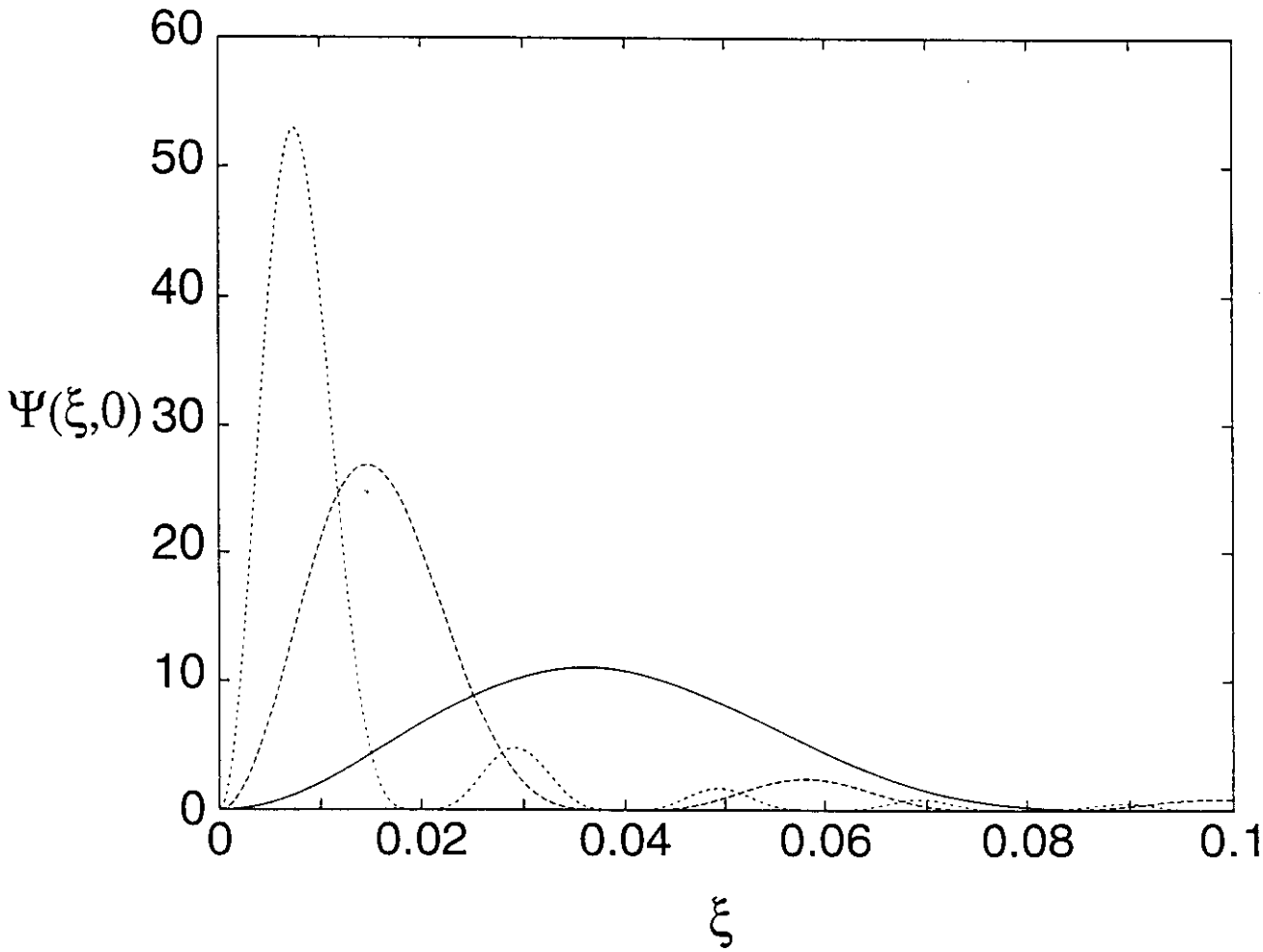

F. Großmann et al. Fig. 1

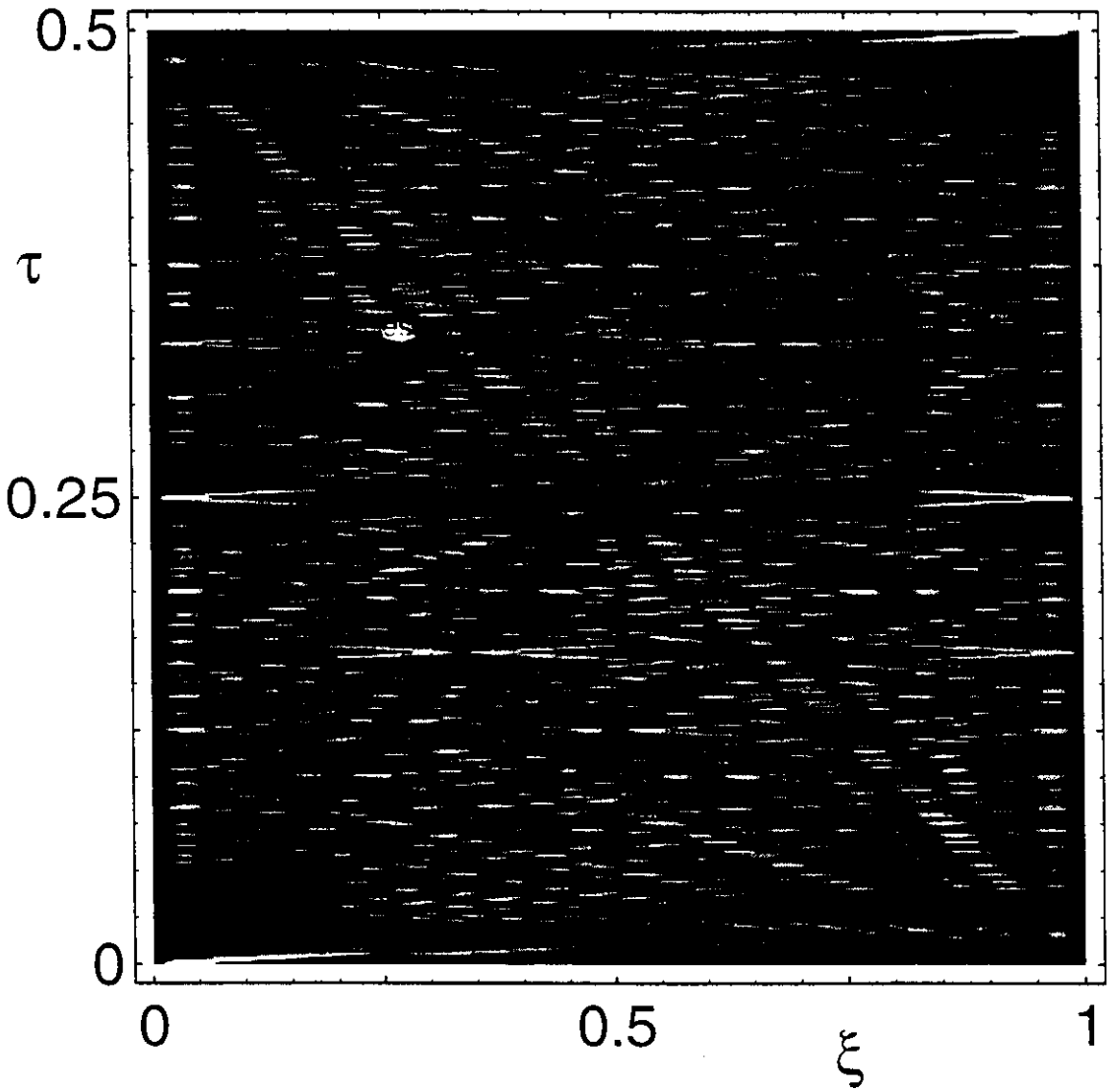

F. Großmann et al. Fig. 2

Generic Structure of Multilevel Quantum Beats

C. Leichtle, I. Sh. Averbukh,* and W. P. Schleich†
Abteilung für Quantenphysik, Universität Ulm, D-89069 Ulm, Germany
(Received 29 January 1996)

Many transient signals from quantum systems result from beats among a large number of levels whose energies depend nonlinearly on the quantum number. Typical examples range from time-resolved laser femtochemistry to quantum optics of single atoms in cavities. Starting from rather general assumptions on the nature of the system, we derive approximate closed-form expressions, which describe such signals in the semiclassical limit. Our approach brings out in a most natural way the phenomenon of fractional revivals and full revivals and explains the oscillatory structures observed in recent experiments on atomic wave packets [Phys. Rev. Lett. **72**, 3783 (1994)]. [S0031-9007(96)01607-9]

PACS numbers: 42.50.Md

Time-dependent signals originating from a large number of simultaneously excited quantum levels appear in the physics of wave packets in atoms [1], molecules [2], and cavity QED [3]. Wave packets explore the correspondence principle at the quantum-classical border [4]. Moreover, this field is closely related to laser femtochemistry [5], which studies molecular dynamics and chemical reactions "in real time." Despite the different physical nature of these systems and the studied signals, there is a surprising similarity [6] in the overall structure of their temporal behavior, as exemplified by Fig. 1 for the case of an atomic wave packet. In addition to the universal feature of fractional revivals and full revivals [7–11] in such transient signals, there is also a certain universality in their fine structure as can be seen from Fig. 1(b).

In the present Letter we introduce for the first time an *analytical* approach towards this universal behavior of beat signals. Our analysis describes not only the shapes of individual peaks, but also reproduces properly the behavior of groups of peaks over a wide time range. We emphasize that the long-time limit of such multilevel quantum beats has only recently become experimentally accessible [8].

For time intervals, in which relaxation is negligible, transient signals such as the one of Fig. 1 are generally of the form [10]

$$S(t) = \sum_n P_n e^{i\omega(n)t} = e^{i\omega(\bar{n})t} S(t) \tag{1}$$

with

$$S(t) = \sum_{m=-\infty}^{\infty} P_{\bar{n}+m} \times \exp\left[2\pi i\left(\frac{t}{T_1}m - \frac{t}{T_2}m^2 + \frac{t}{T_3}m^3 + \cdots\right)\right]. \tag{2}$$

Here we assume that the distribution of weight factors P_n is normalizable, has a dominant maximum at the integer $\bar{n}$ and the width $\Delta n \gg 1$. The characteristic times $T_j = j!\,2\pi/|\omega^{(j)}(\bar{n})|$ follow from the derivatives $\omega^{(j)}$ of the frequencies $\omega(n)$ of the underlying quantum system with respect to n. Note that for definiteness we have chosen the signs of the second and third derivative of ω as in the Coulombic case, where the spectrum reads $E(n) = -R_y/n^2$ with the Rydberg constant $R_y = 13.6$ eV. In the semiclassical limit the natural time scales T_j are well separated and build up a hierarchy $T_1 \ll T_2 \ll T_3 \ll \cdots$.

The temporal behavior of the experimental signal shown in Fig. 1 is not obvious from the *form* of $S(t)$ in Eq. (2). Nevertheless, we can extract the characteristic features by performing an exact transformation of this sum. The key idea of our approach is a decomposition into a number of subsums, each of which contains only terms whose phases are close to each other. We achieve this by combining each rth term of the original sum to one subsum. The particular choice of r depends on the time interval of interest.

Consider, for example, the behavior of $S(t)$ in the neighborhood of the time $t = q/r\,T_2$ where fractional revivals appear [11]. Here q and r are mutually prime integers. It is advantageous to shift the origin of time into the region of $q/r\,T_2$ and choose it to be an integer multiple l of T_1, that is

$$t \equiv lT_1 + \Delta t \equiv \frac{q}{r}T_2 + \epsilon_{q/r}T_1 + \Delta t, \tag{3}$$

where the remainder $|\epsilon_{q/r}| \leq 1/2$. Hence the sum $S(\Delta t) \equiv S(t = q/rT_2 + \epsilon_{q/r}T_1 + \Delta t)$ reads

$$S(\Delta t) = \sum_{m=-\infty}^{\infty} \gamma_m^{(r)} W_m(\Delta t), \tag{4}$$

where

$$\gamma_m^{(r)} \equiv \exp\left(-2\pi i\,\frac{q}{r}\,m^2\right) \tag{5}$$

and

$$W_m(\Delta t) \equiv P_{\bar{n}+m} \exp\left\{2\pi i\left[\frac{\Delta t}{T_1}m - \left(\epsilon_{q/r} + \frac{\Delta t}{T_1}\right)\frac{T_1}{T_2}m^2 + \left(l + \frac{\Delta t}{T_1}\right)\frac{T_1}{T_3}m^3 + \cdots\right]\right\}. \tag{6}$$

0031-9007/96/77(19)/3999(4)$10.00

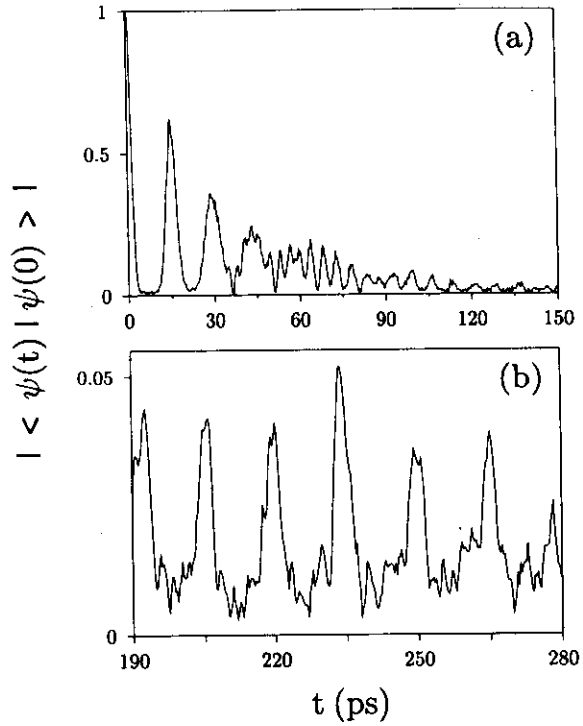

FIG. 1. Experimental data [7] of the autocorrelation function $C(t) = |\langle\psi(t)|\psi(0)\rangle|$ of an atomic wave packet. From (a) we recognize that in the early stage $C(t)$ is almost periodic with a period $T_1 \simeq 15.3$ ps corresponding to the typical energy separation between neighboring eigenstates. However, for larger times this periodicity disappears and new features emerge: At fractions of another characteristic time $T_2 \gg T_1$ the system is again periodic, a phenomenon referred to as fractional revivals. The period is now a fraction of T_1. In the immediate vicinity of the time $T_2 \simeq 474$ ps the signal would even restore almost completely its initial shape giving rise to full revivals. However, the same periodicity occurs near the time point $T_2/2 \simeq 237$ ps as shown in (b), but in this region the signal pattern is shifted by $T_1/2$ with respect to the initial one. These fractional revivals show an asymmetric shape with a fast decay on one side and a slow oscillatory fall down on the other.

Here we have used that according to Eq. (3) $\exp(2\pi imt/T_1) = \exp(2\pi im\Delta t/T_1)$. Note that this representation of the sum S depends on the choice of the origin of time and thus on the fraction q/r. Hence for every different time region under consideration we adopt a different representation of the sum S.

We proceed by noting that the function $\gamma_m^{(r)}$, Eq. (5), is periodic in m with period r, that is $\gamma_{m+r}^{(r)} = \gamma_m^{(r)}$. In order to make use of this periodicity we rearrange the summation with the help of the relation

$$\sum_{m=-\infty}^{\infty} a_m = \sum_{p=0}^{r-1} \sum_{k=-\infty}^{\infty} a_{p+kr}\,. \tag{7}$$

This technique combines those terms to subsums whose phases are close to each other [12]. Since $\gamma_{p+kr}^{(r)} = \gamma_p^{(r)}$, we find

$$S(\Delta t) = \sum_{p=0}^{r-1} \gamma_p^{(r)} \sum_{k=-\infty}^{\infty} W_{p+kr}(\Delta t)\,. \tag{8}$$

We now apply the Poisson summation formula [13]

$$\sum_{k=-\infty}^{\infty} f_k = \sum_{m=-\infty}^{\infty} \int_{-\infty}^{\infty} dk\, f(k) \exp(-2\pi ikm) \tag{9}$$

to the subsums over k in Eq. (8). This allows us to represent the discrete superposition of many harmonics as a sequence of time dependent signals numbered by the index m and arriving one after another. The application of this formula leads to a significant simplification when the width of each signal in time is shorter than the separation between two signals. Indeed we arrive at

$$S(\Delta t) = \sum_{p=0}^{r-1} \gamma_p^{(r)} \sum_{m=-\infty}^{\infty} \times \int_{-\infty}^{\infty} dk\, W(p + kr, \Delta t) \exp(-2\pi ikm)\,, \tag{10}$$

where $W(x, \Delta t)$ is the continuous version of $W_m(\Delta t)$, Eq. (6). When we introduce the new integration variable $x = p + kr$, the integral over x is independent of p, that is

$$S(\Delta t) = \frac{1}{r} \sum_{p=0}^{r-1} \gamma_p^{(r)} \sum_{m=-\infty}^{\infty} \exp\left(2\pi i \frac{p}{r} m\right) \times \int_{-\infty}^{\infty} dx\, W(x, \Delta t) \exp\left(-2\pi i \frac{m}{r} x\right). \tag{11}$$

The interchange of the two summations allows one to write the sum S now in the form

$$S(\Delta t) = \sum_{m=-\infty}^{\infty} \mathcal{W}_m^{(r)} I_m^{(r)}(\Delta t)\,, \tag{12}$$

where

$$\mathcal{W}_m^{(r)} = \frac{1}{r} \sum_{p=0}^{r-1} \exp\left[2\pi i \left(p \frac{m}{r} - p^2 \frac{q}{r}\right)\right] \tag{13}$$

and

$$I_m^{(r)}(\Delta t) = \int_{-\infty}^{\infty} dx\, P(\bar{n} + x) \exp\left\{2\pi i \left[\left(\frac{\Delta t}{T_1} - \frac{m}{r}\right)x - \left(\epsilon_{q/r} + \frac{\Delta t}{T_1}\right)\frac{T_1}{T_2} x^2 + \left(l + \frac{\Delta t}{T_1}\right)\frac{T_1}{T_3} x^3 + \cdots\right]\right\}. \tag{14}$$

The exact representation of the sum S in Eq. (12) is the central result of the paper. It reveals in the most obvious way the revival structure of the signal S, because each fractional revival corresponds to a single term in the sum Eq. (12). Before we illustrate this feature by discussing the functions $\mathcal{W}_m^{(r)}$ and $I_m^{(r)}(\Delta t)$ in more detail, we note that our method also allows one to investigate the full revivals by setting $q = r = 1$.

The function $\mathcal{W}_m^{(r)}$ is independent of the distribution P_n and the time Δt. Thus it acts in the sum Eq. (12) as a weighting factor. Because of the properties of $\mathcal{W}_m^{(r)}$ discussed in Ref. [11], only every second term in the sum Eq. (12) has a nonvanishing value when r is even, whereas for r odd this is true for every value of m.

Now we turn to the discussion of $I_m^{(r)}(\Delta t)$ and its time dependence. To be specific, we use the example of the Coulombic spectrum together with a Gaussian distribution for P_n. In order to be consistent with the experimental data presented in Fig. 1 we choose for the center $\bar{n}$ and the variance Δn of the Gaussian the numerical values $\bar{n} = 46$ and $\Delta n = 2$. Hence the times T_1 and T_2 take on the values $T_1 \simeq 14.8$ ps and $T_2 = 2\bar{n}T_1/3 = 30.67T_1 \simeq 460$ ps. In Fig. 2(a) we show by a dashed curve the behavior of the modulus of the sum Eq. (1) in the vicinity of $t = \frac{1}{2}T_2$, where the fractional revivals of order $\frac{1}{2}$ occur. Here we have evaluated Eq. (1) numerically. We note that this signal shows very similar features as in Fig. 1(b).

We proceed by evaluating $I_m^{(r)}$ for the Coulombic case. We first note that for times t of the order of T_2 we can neglect the quartic term and all higher order terms in the expansion in Eq. (14). In this case we can evaluate the integral $I_m^{(r)}(\Delta t)$ analytically as shown in Ref. [14], which yields

$$I_m^{(r)}(\Delta t) = e^{i\Phi_m(\Delta t)} G(\Delta t) F_m(\Delta t) \mathrm{Ai}[z_m(\Delta t)]. \quad (15)$$

Here the functions $G(\Delta t)$ and $F_m(\Delta t)$ are defined by

$$G(\Delta t) = A \exp\left[-\sigma\left(\epsilon_{q/r} + \frac{\Delta t}{T_1}\right)^2\right] \quad (16)$$

and

$$F_m(\Delta t) = \exp\left[\mu\left(\frac{\Delta t}{T_1} - \frac{m}{r}\right)\right], \quad (17)$$

and $\mathrm{Ai}(z)$ denotes the Airy function of complex argument. The quantities $\Phi_m(\Delta t)$, A, σ, and μ are real whereas $z_m(\Delta t)$ is complex. For the explicit expressions of these quantities we refer to Ref. [14].

We are now in the position to understand the location, shape, and fine structure of each fractional revival shown in Fig. 2(a). For the time region $t \sim T_2/2 = 15.33T_1$, Eq. (3) immediately gives the parameters $q = 1$, $r = 2$, $l = 15$, and hence $\epsilon_{1/2} = -0.33$. Hence the weight factor $\mathcal{W}_m^{(2)}$ takes on the values $|\mathcal{W}_{m=2k}^{(2)}| \equiv 0$ and $|\mathcal{W}_{m=2k+1}^{(2)}| \equiv 1$. Moreover, we find according to Ref. [14] $A = 1.98$, $\sigma = 0.15$, and $\mu = 2.94$.

In Fig. 2(a) we show by a solid line the analytical result, Eq. (12), using Eqs. (15)–(17). We find an excellent agreement between the direct numerical evaluation of the sum S, Eq. (1), and the analytical approximation. In Fig. 2(b) we show by a solid curve the single term $|I_{m=1}^{(2)}(\Delta t)|$ in the sum Eq. (12), together with the Gaussian $G(\Delta t)/A$, the exponential $F_{m=1}(\Delta t)$, and

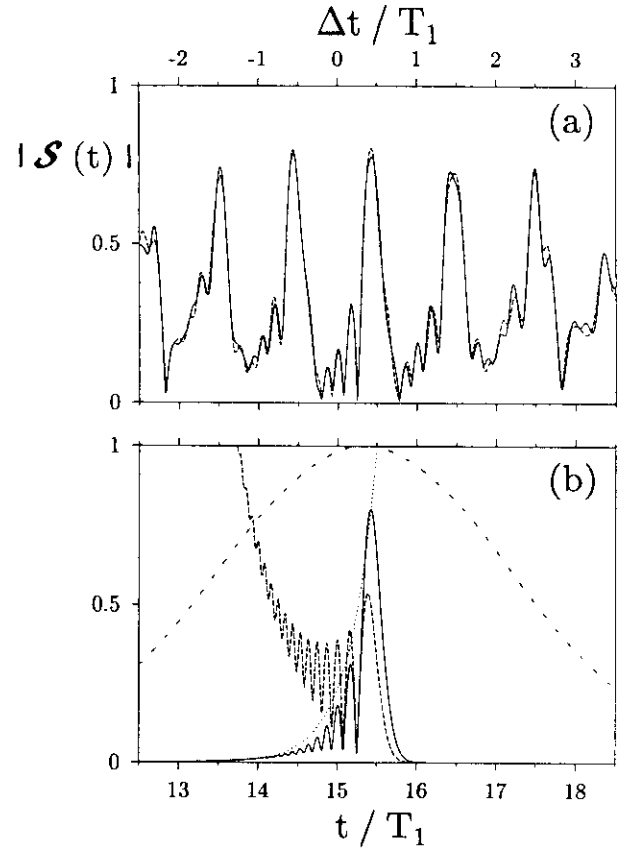

FIG. 2. Fractional revivals of the generic signal $|S(t)|$ for the Coulombic spectrum. In (a) we show by a dashed curve the exact signal Eq. (1) in the neighborhood of $t = \frac{1}{2}T_2 = 15.33T_1$. The solid line shows the signal using the analytical result Eq. (12). We indicate on the top of the figure the relative time Δt introduced in Eq. (3). In (b) we show by a solid line the term $|I_{m=1}^{(2)}(\Delta t)|$, Eq. (15), of the sum Eq. (12). The Gaussian $G(\Delta t)/A$, Eq. (16), the exponential $F_{m=1}(\Delta t)$, Eq. (17), and the absolute value $|\mathrm{Ai}(z_{m=1}(\Delta t))|$ of the complex-valued Airy function are depicted by the dashed, dotted, and broken lines, respectively.

$|\mathrm{Ai}(z_{m=1}(\Delta t))|$. It is the product of the latter two functions, which yields the pronounced peak of $|I_{m=1}^{(2)}(\Delta t)|$ centered at $\Delta t = 0.5T_1$. The Gaussian, which is independent of the index m and centered at $\Delta t = -\epsilon_{1/2}T_1 = 0.33T_1$, just influences the height of the peak, since this function varies very slowly compared to the other two functions. Note that the fine structure of the peak, that is the oscillating structure on its left wing, results exclusively from the Airy function. Figure 2(b) clearly shows that the term $|I_{m=1}^{(2)}(\Delta t)|$ reproduces the fractional revival centered at $t = 15.5T_1$, that is at $\Delta t = 0.5T_1$. Hence there is a one-to-one correspondence between this signal peak and a single term in the sum Eq. (12) [15]. Moreover, the detailed analysis of Ref. [14] shows that a larger value of $|m|$ results in a broader fractional revival centered at $\Delta t_m = m/r\,T_1$ with less pronounced oscillations. This is consistent both with the numerical example of Fig. 2(a) and the experimental data of Fig. 1(a).

When two functions $I_m^{(r)}(\Delta t)$ and $I_{m'}^{(r)}(\Delta t)$ overlap considerably, interferences between these terms in Eq. (12) arise. Then the function $\exp[i\Phi_m(\Delta t)]$ and the phase of the complex Airy function start to play an important role. Consequently, the sum S exhibits a more complicated pattern at the edges of the time window shown in Figs. 1(b) and 2(a). In this regime there is no simple one-to-one correspondence between individual terms in the sum S and the pattern. Nevertheless, Eq. (12) still gives a complete description of the signal S in the vicinity of Δt_m by taking into account only a few terms.

We conclude by noting that the asymmetric oscillations apparent in Fig. 2(b) are a universal feature of transient signals in the long-time limit. They originate from the Airy function which emerges in the most natural way from our theory. The small "forerunner" preceding the main wave packet observed experimentally and explained only numerically in Ref. [7] stems from this Airy function. We can therefore consider this forerunner as a manifestation of "rainbow scattering in the time domain" [16].

In summary, we have presented analytical expressions which describe the generic structure of signals originating from a large number of simultaneously excited quantum levels. A new representation of the underlying sum allowed us for the first time to treat analytically the influence of higher order dispersion effects on quantum beats. The influence of the third order term has already been observed in Ref. [7] in atomic wave packets. The experimental tools in this field have become so refined that even higher order corrections included in our treatment will soon be observed. Moreover, the recent experimental realization of the Jaynes-Cummings model [9] describing the motion of an ion in a Paul trap provides another arena for probing generic structures in the long-time limit of quantum beats.

We enjoyed many stimulating discussions with V. M. Akulin, M. V. Berry, and M. Nauenberg, and thank H. B. van Linden van den Heuvell and J. Wals for many fruitful conversations and for providing us with the experimental data shown in Fig. 1. One of us (I. A.) appreciates the kind hospitality and support at the Universität Ulm. C. L. thanks the Deutsche Forschungsgemeinschaft for its support and acknowledges the warm hospitality during his stay at the Weizmann Institute of Science, Rehovot.

*Also Weizmann Institute of Science, Rehovot, 76100, Israel.

†Also Max-Planck-Institut für Quantenoptik, D-85748 Garching, Germany.

[1] For a review, see, e.g., G. Alber and P. Zoller, Phys. Rep. **199**, 231 (1990).

[2] For a review, see, e.g., M. Gruebele and A. Zewail, Phys. Today **43**, 24 (1990); B. M. Garraway and K.-A. Suominen, Rep. Prog. Phys. **58**, 365 (1995).

[3] J. H. Eberly *et al.*, Phys. Rev. Lett. **44**, 1323 (1980).

[4] M. Nauenberg *et al.*, Sci. Am. **270**, No. 6, 24 (1994), and references therein; M. Nauenberg, Comments At. Mol. Phys. **25**, 151 (1990).

[5] A. H. Zewail, *Femtochemistry* (World Scientific, Singapore, 1994), Vols. 1 and 2.

[6] General aspects of the dynamics of wave packets in atomic, molecular, and quantum optical systems are discussed in a review article by I. Sh. Averbukh and N. F. Perel'man, Sov. Phys. Usp. **34**, 572 (1991).

[7] J. Wals *et al.*, Phys. Rev. Lett. **72**, 3783 (1994); J. Wals *et al.*, Physica Scr. **T58**, 62 (1995).

[8] For the experimental observation of fractional revivals and full revivals of atomic wave packets, see, e.g., J. A. Yeazell *et al.*, Phys. Rev. Lett. **64**, 2007 (1990); J. A. Yeazell and C. R. Stroud, Jr., Phys. Rev. A **43**, 5153 (1991); D. R. Meacher *et al.*, J. Phys. B **24**, L63 (1991); L. Marmet *et al.*, Phys. Rev. Lett. **72**, 3779 (1994); G. Raithel *et al.*, J. Phys. B **27**, 2849 (1994). For molecular wave packets, see T. Baumert *et al.*, Chem. Phys. Lett. **191**, 639 (1992); I. Fischer *et al.*, J. Chem. Phys. **102**, 5566 (1995); M. J. J. Vrakking *et al.*, Phys. Rev. A **54**, R37 (1996).

[9] For the experimental observation of "Jaynes-Cummings (J-C) revivals" in cavity QED, see G. Rempe *et al.*, Phys. Rev. Lett. **58**, 353 (1987); M. Brune *et al.*, Phys. Rev. Lett. **76**, 1800 (1996); in Paul traps, see D. M. Meekhof *et al.*, Phys. Rev. Lett. **76**, 1796 (1996). Note, however, that these "J-C revivals" are a short-time phenomenon and occur at integer multiples of T_1. They therefore correspond to the T_1-periodic behavior of the autocorrelation function of Fig. 1(a). In contrast, the revivals as defined in Refs. [7,8,10,11] occur at $T_2 \gg T_1$ and have not yet been observed experimentally for the Jaynes-Cummings model.

[10] J. Parker and C. R. Stroud, Jr., Phys. Rev. Lett. **56**, 716 (1986).

[11] I. Sh. Averbukh and N. F. Perel'man, Phys. Lett. A **139**, 449 (1989); Sov. Phys. JETP **69**, 464 (1989).

[12] This technique has also been used to treat the integer, fractional, and fractal Talbot effect, see M. V. Berry, J. Phys. A (to be published); M. V. Berry and S. Klein, J. Mod. Optics (to be published); see also J. T. Winthrop and C. R. Worthington, J. Opt. Soc. Am. **49**, 372 (1965).

[13] R. Courant and D. Hilbert, *Methods of Mathematical Physics* (Interscience Publishers, New York, 1953).

[14] C. Leichtle *et al.*, Phys. Rev. A (to be published).

[15] This fact may be used to extract the local parameters of the spectrum by fitting Eq. (15) to experimental data of a *single* (fractional) revival.

[16] For rainbow scattering, see, for example, M. V. Berry and K. E. Mount, Rep. Prog. Phys. **35**, 315 (1972).

Endoscopy in the Paul Trap: Measurement of the Vibratory Quantum State of a Single Ion

P. J. Bardroff, C. Leichtle, G. Schrade, and W. P. Schleich*
Abteilung für Quantenphysik, Universität Ulm, D-89069 Ulm, Germany
(Received 25 April 1996)

We reconstruct the density operator of the center-of-mass motion of an ion stored in a Paul trap by mapping the dynamics of the motion onto the internal dynamics of the ion. Our technique takes into account the explicit time dependence of the trap potential, operates outside the Lamb-Dicke limit, and is not restricted to pure states. We demonstrate the feasibility of this method using the example of a damped Schrödinger cat state. [S0031-9007(96)01127-1]

PACS numbers: 32.80.Pj, 03.65.Bz, 42.50.Vk

The recent experimental generation [1,2] of nonclassical states of the motion of an ion in a Paul trap [3] has propelled the field of quantum state preparation [4,5] into a new era. But how can we prove that the ion is indeed in a Fock, a squeezed, or a Schrödinger cat state? How can we measure a motional state which, due to the explicit time dependence of the binding force of the Paul trap, displays [6] a complicated time dependence? In this Letter we present the first method [7] that measures a vibratory state of an ion taking into account the complete time dependence of the Paul trap. Moreover, our technique operates outside the Lamb-Dicke regime [8] and is not limited to pure states only.

The central idea of our approach is to map the dynamics of the center-of-mass motion onto the internal degrees of the ion. The dynamics of the latter we can read out using quantum jumps [9]. Three techniques make this approach possible: (i) the well-known Floquet solution [10] of the harmonic oscillator with time-dependent frequency, (ii) the rotating wave approximation [11] resulting in a time independent s-phonon Jaynes-Cummings interaction Hamiltonian between the center-of-mass motion and the internal states of the ion [12], and (iii) the application of quantum state endoscopy [13,14] originally devised for the measurement of a field state to the problem at hand. We demonstrate the feasibility of Paul trap endoscopy using the example of a damped Schrödinger cat state.

We start from the Hamiltonian

$$\hat{H}(t) = \hat{H}_a + \hat{H}_{\rm cm}(t) + \hat{H}_{\rm int}(t) \tag{1}$$

of a single two-level ion moving along one direction in a Paul trap and interacting with a classical laser field, where $\hat{H}_a = \frac{1}{2}\hbar\omega_a\hat{\sigma}_z$ describes the two internal states with transition frequency ω_a and $\hat{\sigma}_z$ is the Pauli matrix.

The one-dimensional center-of-mass motion of an ion with mass m in a harmonic potential with time-dependent steepness

$$\omega^2(t) = \tfrac{1}{4}\omega_{\rm rf}^2[a + 2q\cos(\omega_{\rm rf}t)] \tag{2}$$

follows from the Hamiltonian

$$\hat{H}_{\rm cm}(t) = \tfrac{1}{2m}\hat{p}^2 + \tfrac{1}{2}m\omega^2(t)\hat{x}^2 . \tag{3}$$

The dimensionless parameters a and q are proportional [3] to the dc and ac voltages applied to the trap, respectively, and $\omega_{\rm rf} \equiv 2\pi/T$ is the frequency of the ac voltage.

In the rotating wave approximation we model the interaction of the classical laser field with the two levels of the ion by the Hamiltonian [15]

$$\hat{H}_{\rm int}(t) = \hbar g\{\hat{\sigma}^+ \exp[-i(\omega_L t - k\hat{x})] + \text{H.c.}\}, \tag{4}$$

where g and k denote the interaction strength and the wave vector of the light field with frequency ω_L, respectively. The Pauli matrix $\hat{\sigma}^+$ is the raising operator for the internal levels of the ion. Hence the laser field couples the center-of-mass motion to the internal states.

In order to solve the Schrödinger equation $i\hbar|\dot{\Psi}\rangle = \hat{H}(t)|\Psi\rangle$ for the state vector $|\Psi(t)\rangle$ describing both the internal states and the center-of-mass motion it is convenient to work in the interaction picture. We recall the relation [16]

$$\tilde{\hat{x}}(t) \equiv \hat{U}_{\rm cm}^\dagger(t)\hat{x}\hat{U}_{\rm cm}(t) = \sqrt{\tfrac{\hbar}{2m\omega_r}}[\epsilon^*(t)\hat{b} + \epsilon(t)\hat{b}^\dagger], \tag{5}$$

where $\hat{U}_{\rm cm}(t) = \hat{T}\exp[-\frac{i}{\hbar}\int_0^t dt'\hat{H}_{\rm cm}(t')]$ is the propagator of the center-of-mass motion, $\hat{T}$ is the time-ordering operator, and operators with a tilde are in the interaction picture. We denote the annihilation and creation operators of a time independent reference harmonic oscillator [10,17] with frequency ω_r by $\hat{b}$ and $\hat{b}^\dagger$. Note that the reference frequency ω_r is an arbitrary real parameter, which we choose later in a convenient way. The complex function $\epsilon(t)$ satisfies the classical Mathieu differential equation

$$\ddot{\epsilon}(t) + \omega^2(t)\,\epsilon(t) = 0 \tag{6}$$

with the initial conditions $\epsilon(0) = 1$ and $\dot{\epsilon}(0) = i\,\omega_r$.

To bring out most clearly that the laser field induces transitions between the energy eigenstates $|n\rangle$ of the time-independent reference oscillator we express the center-of-mass motion part of the interaction Hamiltonian equation (4) in these states. Indeed the interaction Hamiltonian

$$\tilde{\hat{H}}_{\rm int}(t) = \sum_{n=0}^{\infty}\sum_{s=-n}^{\infty}\hbar\Omega^{(n,n+s)}(t)\hat{\sigma}^+|n\rangle\langle n+s| + \text{H.c.} \tag{7}$$

 0031-9007/96/77(11)/2198(4)$10.00

in the interaction picture involves all possible s-phonon transitions [12]. The time-dependent frequencies $\Omega^{(n,n+s)}(t) \equiv g e^{-i\Delta t}\langle n|\hat{D}[\alpha(t)]|n+s\rangle$ follow from Eq. (4) with the help of Eq. (5). They involve the matrix elements of the displacement operator $\hat{D}(\alpha) \equiv \exp(\alpha\hat{b}^\dagger - \alpha^*\hat{b})$ at the complex valued time-dependent displacement $\alpha(t) \equiv i\eta\epsilon(t)$, where $\eta \equiv k[\hbar/(2m\omega_r)]^{1/2}$ denotes the Lamb-Dicke parameter. Here $\Delta \equiv \omega_L - \omega_a$ is the detuning between the laser frequency and the atomic transition frequency. When we evaluate [18] the matrix element $\langle n|\hat{D}[\alpha(t)]|n+s\rangle$ the frequencies $\Omega^{(n,n+s)}(t)$ read for $s \geq 0$

$$\Omega^{(n,n+s)}(t) = g\left[\frac{n!}{(n+s)!}\right]^{1/2} \exp(-i\Delta t)[i\eta\epsilon^*(t)]^s \times \exp\left[-\frac{\eta^2}{2}|\epsilon(t)|^2\right] L_n^s(\eta^2|\epsilon(t)|^2). \quad (8)$$

Here L_n^s denotes the generalized Laguerre polynomial. Similar relations hold for $s < 0$.

We note that the time dependence of $\Omega^{(n,n+s)}(t)$ results from the detuning Δ and the complex valued function $\epsilon(t)$. In order to simplify this time dependence and hence the interaction Hamiltonian equation (7) we focus on the so-called Floquet solution

$$\epsilon^{(F)}(t) = \exp(i\mu t)\phi(t). \quad (9)$$

Here the characteristic exponent μ and the periodic function

$$\phi(t) = \phi(t+T) = \sum_{n=-\infty}^{\infty} c_n \exp(in\omega_{\rm rf}t) \quad (10)$$

are determined [10] by the trap parameters a and q. In the stable region of the Mathieu equation [19] the expansion coefficients c_n and the characteristic exponent μ are purely real. Then the frequency μ gives the secular frequency of the motion of the ion. Note that it is the specific choice [10]

$$\omega_r^{(F)} = \mu + \omega_{\rm rf}\sum_{n=-\infty}^{\infty} n c_n \quad (11)$$

of the reference frequency ω_r as the initial condition $\dot{\epsilon}(0) = i\omega_r^{(F)}$, which enforces the quasiperiodic solution Eq. (9) of the differential equation (6).

We substitute the Floquet solution $\epsilon^{(F)}(t)$, Eq. (9), into the time-dependent frequencies Eq. (8) and arrive at

$$\Omega^{(n,n+s)}(t) = \sum_{l=-\infty}^{\infty} \omega_l^{(n,n+s)} \exp[i(l\omega_{\rm rf} - s\mu - \Delta)t],$$

where the coefficients

$$\omega_l^{(n,n+s)} \equiv g\left[\frac{n!}{(n+s)!}\right]^{1/2}(i\eta)^s \times \int_{-T/2}^{T/2}\frac{dt}{T}[\phi^*(t)]^s e^{-\eta^2|\phi(t)|^2/2} \times L_n^s(\eta^2|\phi(t)|^2)e^{-il\omega_{\rm rf}t} \quad (12)$$

follow by expanding the part of $\Omega^{(n,n+s)}$ in Fourier series, which is periodic in $T = 2\pi/\omega_{\rm rf}$. When we now use this expression for $\Omega^{(n,n+s)}$ the interaction Hamiltonian in the interaction picture reads

$$\hat{\tilde{H}}_{\rm int}(t) = \sum_{n=0}^{\infty}\sum_{s=-n}^{\infty}\sum_{l=-\infty}^{\infty}\hbar\omega_l^{(n,n+s)} \times \exp[i(l\omega_{\rm rf} - s\mu - \Delta)t] \times \hat{\sigma}^+|n\rangle\langle n+s| + \text{H.c.} \quad (13)$$

We emphasize that this representation is exact. It shows that the time dependence of $\hat{\tilde{H}}_{\rm int}(t)$ is governed by the specific combination $l\omega_{\rm rf} - s\mu - \Delta$ of all harmonics of the frequency $\omega_{\rm rf}$ and of the secular frequency μ, and the detuning Δ. This feature allows us to perform a time average [11] of $\hat{\tilde{H}}_{\rm int}(t)$ in order to obtain an s_0-phonon Hamiltonian as we show now.

So far we have not yet specified the detuning Δ. We choose it in such a way that one of the terms in the sums in Eq. (13) is slowly varying, whereas all the others are rapidly oscillating. This happens when $s_0\mu + \Delta \equiv l_0\omega_{\rm rf}$. Note that this condition leads to an interesting number theoretical problem. In order to achieve a large coupling to the field we choose Δ such that only the term with the largest coefficient $\omega_{l_0}^{(n,n+s_0)}$ survives the time averaging for s_0 fixed. Hence we choose $\Delta = l_0\omega_{\rm rf} - s_0\mu$ provided that $\Delta + s\mu$ is not a multiple integer of the frequency $\omega_{\rm rf}$ for all $s \neq s_0$. With the help of the rotating wave approximation we therefore arrive at the time averaged Hamiltonian

$$\hat{\tilde{H}}_{\rm int} = \sum_{n=0}^{\infty}\hbar\omega_{l_0}^{(n,n+s_0)}\hat{\sigma}^+|n\rangle\langle n+s_0| + \text{H.c.}, \quad (14)$$

which is the s_0-phonon Jaynes-Cummings Hamiltonian.

Since we face the Jaynes-Cummings Hamiltonian, we can use the method of quantum state endoscopy [13,14] and reconstruct the initial vibrational density operator $\hat{\rho}(0)$ of the ion from the measured time evolution of its internal state. For the application of this method we use the coherent superposition $|\Psi_a\rangle = (|e\rangle + e^{i\varphi}|g\rangle)/\sqrt{2}$ of the excited and the ground state as initial internal state. We then can extract from the probability

$$P_e(t;\varphi) \equiv \text{Tr}_{\rm cm}\langle e|e^{-i\hat{\tilde{H}}_{\rm int}t/\hbar}[\hat{\rho}(0)\otimes|\Psi_a\rangle\langle\Psi_a|]e^{i\hat{\tilde{H}}_{\rm int}t/\hbar}|e\rangle = \tfrac{1}{2} - \tfrac{1}{4}\sum_{n=0}^{s_0-1}\rho_{n,n} + \tfrac{1}{4}\sum_{n=0}^{\infty}\cos(2\omega_{l_0}^{(n,n+s_0)}t)(\rho_{n,n} - \rho_{n+s_0,n+s_0}) - \tfrac{1}{2}\sum_{n=0}^{\infty}\sin(2\omega_{l_0}^{(n,n+s_0)}t)\text{Im}[(-i)^{s_0}\rho_{n,n+s_0}e^{-i\varphi}]$$

of finding the ion in the excited state $|e\rangle$ the matrix elements $\rho_{n,n+s_0} = \langle n|\hat{\rho}(0)|n+s_0\rangle$ of the density operator of the center-of-mass motion. Following Ref. [14], we measure the internal dynamics, that is, $P_e(t;\varphi)$, for two different phases φ, N interaction times, and $s_{\max}$ detunings. Here N and $s_{\max}$ denote the dimensions over which

the density matrix has significant elements. The algorithm of Ref. [14] then allows us to reconstruct from these data the full density matrix.

We demonstrate the feasibility of the reconstruction scheme using as the initial center-of-mass density operator $\hat{\rho}(0)$ a damped Schrödinger cat state

$$\hat{\rho}(0) = p\hat{\rho}_{\text{incoh}}(\alpha) + (1 - p)\hat{\rho}_{\text{cat}}(\alpha). \quad (15)$$

Here p is a weight factor,

$$\hat{\rho}_{\text{incoh}}(\alpha) = \tfrac{1}{2}[|\alpha\rangle\langle\alpha| + |-\alpha\rangle\langle-\alpha|]$$

is a incoherent superposition of two coherent states, and

$$\hat{\rho}_{\text{cat}}(\alpha) = \frac{|\mathcal{N}|^2}{2}[|\alpha\rangle - |-\alpha\rangle][\langle\alpha| - \langle-\alpha|]$$

is a Schrödinger cat state with normalization constant $\mathcal{N}$. Note that we have chosen the coherent state $|\alpha\rangle$ with respect to the time-independent reference oscillator with frequency $\omega_r^{(F)}$. We emphasize that Ref. [2] reported the birth of Schrödinger cats of this kind.

For the numerical simulation of Paul trap endoscopy we use the parameters $p = 0.5$ and $\alpha = 1.5$. Since in this case the Schrödinger cat lies on the real axis, the matrix elements $\rho_{n,m}$ are real. Moreover, we take the trap parameters $a = 0$, $q = 0.4$, and $\eta = 1$. In order to simulate experimental uncertainties in a simple way and to test the stability of the reconstruction procedure, we round the calculated values of $P_e(t;\varphi)$ to the precision of one-tenth.

In Fig. 1(a) we show the relevant matrix elements $\rho_{n,m}$ of the exact density operator Eq. (15). Note that the matrix elements of the reconstructed density operator $\hat{\rho}^{(r)}$ become complex. In Figs. 1(b) and 1(c) we show the real part and the imaginary part of its elements, respectively. We emphasize that there is an excellent agreement between the exact and reconstructed density matrix as is apparent from Figs. 1(c) and 1(d) where we show the difference between the exact and the reconstructed matrix elements in their imaginary and real parts.

The present treatment takes into account the complete time dependence of the trap potential. To bring out the importance of this time dependence, we now compare our exact treatment to the effective potential approximation [15]. The latter describes the vibrational degree of freedom in the limit $a, q \to 0$ by an effective, time-independent harmonic oscillator with frequency μ. In this case, Eq. (10) simplifies to $\phi(t) \simeq 1$, and hence Eq. (9) reduces to $\epsilon^{(F)}(t) \simeq e^{i\mu t}$. As a consequence, the Rabi frequencies $\omega_l^{(n,n+s)}$ Eq. (12) all vanish except for $l \equiv 0$ which read [12]

$$\omega_{\text{eff}}^{(n,n+s)} = g\left[\frac{n!}{(n+s)!}\right]^{1/2}(i\eta)^s e^{-\eta^2/2}L_n^s(\eta^2). \quad (16)$$

In Fig. 2 we show the effective Rabi frequencies $\omega_{\text{eff}}^{(n,n+1)}$ of the one-phonon transition by crosses and compare it to the exact frequencies $\omega_{l=0}^{(n,n+1)}$ for the trap parameters $a = 0$ and the three different values $q = 0.01$ (diamonds), $q = 0.2$ (triangles), and $q = 0.4$ (squares). These parameters are often used [1,2,20] in experiments. For this figure we have chosen the Lamb-Dicke parameter $\eta = 1$. To guide the eye we have connected the discrete values by continuous curves. Whereas for the small value $q = 0.01$ the frequencies almost coincide, we find considerable differences for the values $q = 0.2$ and 0.4. In these cases the differences between the exact and the effective Rabi frequencies are of the same order as the differences between neighboring Rabi

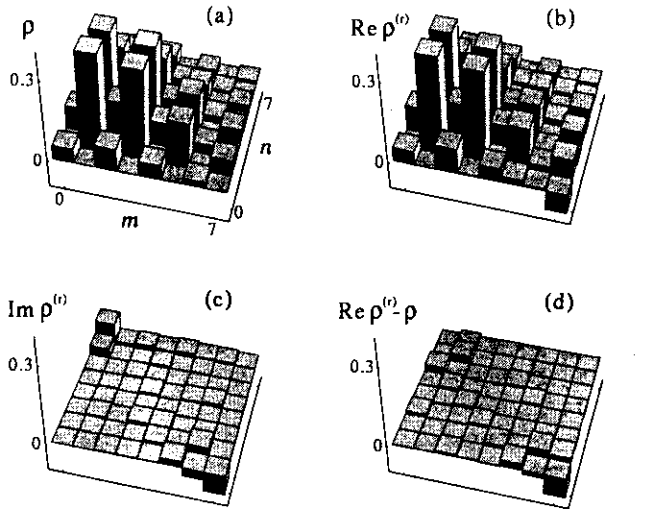

FIG. 1. Paul trap endoscopy illustrated by a damped Schrödinger cat. In (a) we show the matrix elements $\rho_{n,m}$ in energy representation of the cat to be reconstructed. All matrix elements are real. In (b) and (c) we display the real and imaginary parts of the reconstructed matrix elements $\rho_{n,m}^{(r)}$. The tiny differences between the two density matrices in their real and imaginary parts as shown in (d) and (c) demonstrate the feasibility of Paul trap endoscopy.

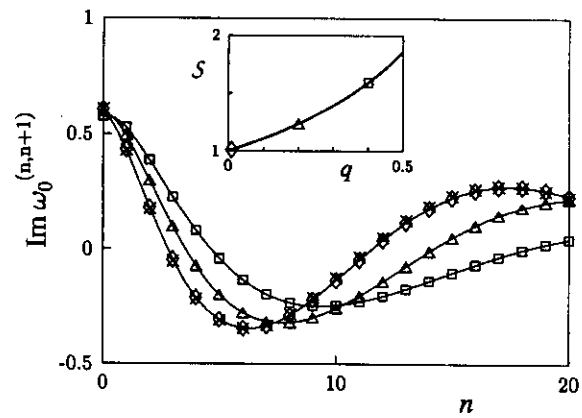

FIG. 2. Comparison between the Rabi frequencies $\omega_{\text{eff}}^{(n,n+1)}$ within the effective potential approximation (crosses) and the exact frequencies $\omega_0^{(n,n+1)}$ including the micromotion for the trap parameters $a = 0$ and three different values of q. Note that according to Eqs. (12) and (16) these frequencies are purely imaginary. The diamonds correspond to $q = 0.01$, the triangles to $q = 0.2$, and the squares to $q = 0.4$. The inset shows the squeezing parameter S for $a = 0$ as a function of q.

frequencies. However, for reconstructing the density operator, it is crucial to distinguish neighboring Rabi frequencies. Hence the influence of the micromotion is not negligible for these values of q.

Another consequence of the effective potential approximation is that the states $|n\rangle$ represent now the energy eigenstates $|n\rangle_\mu$ of the static oscillator with frequency μ. The two different sets of basis states corresponding to the two oscillators with frequencies $\omega_r^{(F)}$ and μ are connected by the squeezing operation $\hat{S}(r) = \exp[r(\hat{b}^{\dagger 2} - \hat{b}^2)/2]$ characterized by the parameter r. It is the ratio $S = \mu/\omega_r^{(F)} = \exp(2r)$ which determines the magnitude of squeezing. In the inset of Fig. 2 we show this ratio as a function of q for $a = 0$. Again the diamond, triangle, and square correspond to the value for $q = 0.01$, 0.2, and 0.4, respectively.

We conclude by summarizing our main results. We have presented a technique that allows us to measure the quantum state of the center-of-mass motion of an ion moving in a Paul trap. In contrast to related work [7] our scheme takes the explicit time dependence of the Paul trap into account. This time dependence might also be relevant for the recent discussions on quantum gates [21] and the quantum computer [22] resulting from many ions stored in a linear trap. We note that our method operates outside of the Lamb-Dicke limit. Moreover, we emphasize that the method is not limited to pure states only. Using the example of a damped Schrödinger cat we have shown that it is possible to perform endoscopy in the Paul trap.

We thank I. Sh. Averbukh, S.L. Braunstein, I. Cirac, H.J. Kimble, R.L. de Matos Filho, O.V. Man'ko, V.I. Man'ko, W. Vogel, S. Wallentowitz, and P. Zoller for fruitful discussions. In particular, we thank D. Leibfried for sending us a preprint of Ref. [23]. We (P.J.B. and C.L.) gratefully acknowledge the support of the DFG.

Note added.—After the completion of this work we have learned that the Boulder group [23] has indeed measured the quantum state of the motion of an ion in a Paul trap.

*Also at Max-Planck-Institut für Quantenoptik, D-85748 Garching, Germany.

[1] D.M. Meekhof *et al.*, Phys. Rev. Lett. **76**, 1796 (1996).
[2] C. Monroe *et al.*, Science **272**, 1131 (1996).
[3] W. Paul, Rev. Mod. Phys. **62**, 531 (1990).
[4] For the preparation of field states, see K. Vogel *et al.*, Phys. Rev. Lett. **71**, 1816 (1993); A.S. Parkins *et al.*, Phys. Rev. Lett. **71**, 3095 (1993); C.K. Law and J.H. Eberly, Phys. Rev. Lett. **76**, 1055 (1996).
[5] For the preparation of states of the motion, see J.I. Cirac *et al.*, Phys. Rev. Lett. **70**, 556 (1993); J.I. Cirac *et al.*, Phys. Rev. Lett. **70**, 762 (1993); R.L. de Matos Filho and W. Vogel, Phys. Rev. Lett. **76**, 608 (1996).
[6] G. Schrade *et al.*, Quant. Semiclass. Opt. **7**, 307 (1995).
[7] For the measurement of the motional state in the time independent effective harmonic potential, see S. Wallentowitz and W. Vogel, Phys. Rev. Lett. **75**, 2932 (1995); J.F. Poyatos *et al.*, Phys. Rev. A **53**, R1966 (1996); C. D'Helon and G.J. Milburn, Phys. Rev. A **54**, R25 (1996).
[8] The Lamb-Dicke limit arises when the characteristic length of the quantum mechanical state of the motion is small compared to the wave length of the light field. See the original papers by W.E. Lamb, Phys. Rev. **51**, 187 (1937); R.H. Dicke, Phys. Rev. **89**, 472 (1953).
[9] W. Nagourney *et al.*, Phys. Rev. Lett. **56**, 2797 (1986); T. Sauter *et al.*, Phys. Rev. Lett. **57**, 1696 (1986); J.C. Bergquist *et al.*, Phys. Rev. Lett. **57**, 1699 (1986).
[10] R.J. Glauber, in *Laser Manipulation of Atoms and Ions*, Proceedings of the International School of Physics "Enrico Fermi," Course CXVIII (Varenna, July, 1992), edited by E. Arimondo *et al.* (North-Holland, Amsterdam, 1992).
[11] In the context of laser cooling, a similar time averaging was used by J.I. Cirac *et al.*, Phys. Rev. A **49**, 421 (1994). However, their analysis focused on the Lamb-Dicke limit only.
[12] W. Vogel and R.L. de Matos Filho, Phys. Rev. A **52**, 4214 (1995).
[13] W. Vogel *et al.*, J. Opt. Soc. Am. B **4**, 1633 (1987).
[14] P.J. Bardroff *et al.*, Phys. Rev. A **51**, 4963 (1995); P.J. Bardroff *et al.*, Phys. Rev. A **53**, 2736 (1996).
[15] C.A. Blockley *et al.*, Europhys. Lett. **17**, 509 (1992).
[16] See, for example, Ref. [11], Eq. (A2).
[17] V.V. Dodonov and V.I. Man'ko, in *Invariants and the Evolution of Nonstationary Quantum Systems*, edited by M.A. Markov (Novo Science, New York, 1989).
[18] K.E. Cahill and R.J. Glauber, Phys. Rev. **177**, 1857 (1969).
[19] M. Abramowitz and I.A. Stegun, *Handbook of Mathematical Functions* (Dover, New York, 1972).
[20] R. Blümel *et al.*, Phys. Rev. A **40**, 808 (1989).
[21] C. Monroe *et al.*, Phys. Rev. Lett. **75**, 4714 (1995).
[22] J.I. Cirac and P. Zoller, Phys. Rev. Lett. **74**, 4091 (1995).
[23] D. Leibfried *et al.* (to be published).

Quantum State Endoscopy: Measurement of the Quantum State in a Cavity

P. J. Bardroff, E. Mayr, and W. P. Schleich
Abteilung für Quantenphysik, Universität Ulm, D-89069 Ulm, Germany
(Received 16 September 1994)

We propose a new measurement scheme to determine the complete state of a single mode of the quantized electromagnetic field in a cavity.

PACS number(s): 42.50.-p, 03.65.Bz, 42.52.+x

Endoscopy [1] in medicine allows to examine hollow organs inside the body. In quantum optics we face a similar task: How to measure the internal structure of a quantum state of the radiation field [2–6] *inside* a resonator? To couple the light out of the cavity is out of the question, since this procedure would drastically alter the quantum state. In the present paper we propose a simple and efficient method to measure the field state in a cavity – quantum state endoscopy.

Our probe is a beam of two-level atoms interacting with the resonant quantized light field as shown in Fig. 1. The atoms enter the cavity in a coherent superposition

$$|\Psi_{\rm A}(t=0)\rangle = \frac{1}{\sqrt{2}}\Big(|a\rangle + e^{i\varphi}|b\rangle\Big) \tag{1}$$

of excited state $|a\rangle$ and ground state $|b\rangle$. We measure the number of atoms exiting the cavity in the excited state as a function of the interaction time. We record this curve for four distinct internal phases φ of the atom. From these data we extract the initial field state

$$|\Psi_{\rm F}(t=0)\rangle = \sum_{n=0}^{\infty} w_n |n\rangle, \tag{2}$$

that is the in general complex-valued photon number probability amplitudes w_n by a simple mathematical algorithm. We show using the parameters of current experiments [7–9] that the proposed measurement technique can be performed today. Our scheme neither needs a complicated setup, nor do we have to perform a difficult data analysis.

We now calculate the probability $P_a(t,\varphi)$ to find the atom in the excited state after an interaction time t when initially the atom was in a superposition state, Eq. (1), of phase difference φ. We describe the resonant interaction of the two level atom and the single mode of a quantized standing light field by the well known Jaynes-Cummings model [10] and neglect spontaneous emission [11]. In rotating wave approximation the Hamiltonian in the interaction picture reads

$$\hat{H}_{\rm int} = \hbar g\left(\hat{\sigma}^{+}\hat{a} + \hat{\sigma}^{-}\hat{a}^{\dagger}\right), \tag{3}$$

where g is the vacuum Rabi frequency. The operators $\hat{\sigma}^{+}$ and $\hat{\sigma}^{-}$ are the Pauli spin operators describing transitions between the atomic states and $\hat{a}^{\dagger}$ and $\hat{a}$ are the creation and annihilation operators of the quantized field. The initial state

$$|\Psi_{\rm A+F}(t=0)\rangle = \frac{1}{\sqrt{2}}\sum_{n=0}^{\infty} w_n\Big(|a,n\rangle + e^{i\varphi}|b,n\rangle\Big) \tag{4}$$

of the combined system of atom plus field is a direct product of the atomic superposition state, Eq. (1), and the field state, Eq. (2). Solving the Schrödinger equation with the interaction Hamiltonian, Eq. (3), subject to the initial condition, Eq. (4), the state of the combined system after the interaction time t reads [10]

$$|\Psi_{\rm A+F}(t)\rangle = \sum_{n=0}^{\infty}\Big(\psi_{a,n}(t)|a,n\rangle + \psi_{b,n+1}(t)|b,n+1\rangle\Big) + \psi_{b,0}(t)|b,0\rangle \tag{5}$$

with the probability amplitudes

$$\psi_{a,n}(t) = \frac{1}{\sqrt{2}}\Big[\cos(\Omega_n t)\, w_n - i\sin(\Omega_n t)\, e^{i\varphi} w_{n+1}\Big]$$

and

$$\psi_{b,n+1}(t) = \frac{1}{\sqrt{2}}\Big[-i\sin(\Omega_n t)\, w_n + \cos(\Omega_n t)\, e^{i\varphi} w_{n+1}\Big],$$

where $\Omega_n \equiv \sqrt{n+1}\, g$. From Eq. (5) we immediately get the probability

$$P_a(t,\varphi) = \frac{1}{2} - \frac{1}{4}|w_0|^2 + \frac{1}{4}\sum_{n=0}^{\infty}\cos(2\Omega_n t)\left(|w_n|^2 - |w_{n+1}|^2\right) - \frac{1}{2}\sum_{n=0}^{\infty}\sin(2\Omega_n t)\,{\rm Im}\left(w_n w_{n+1}^{*} e^{-i\varphi}\right) \tag{6}$$

to find the atom after the interaction time t in the excited state $|a\rangle$, independent of the final field state. But how to extract the initial quantum state of the field out of the measured quantity $P_a(t,\varphi)$? To answer this question we have a closer look at the contributions to P_a: there are (i) two time independent terms, (ii) a contribution of cosine and (iii) the sine of the Rabi frequencies Ω_n. We note that the cosine contribution contains only the absolute values squares of the probability amplitudes. However, due to the presence of the atomic superposition, the sine contribution brings in the relative phase between neighboring photon number probability amplitudes. Hence in order to reconstruct the phases of w_n we have to distill the complex valued product $w_n w_{n+1}^{*}$ out of $P_a(t,\varphi)$. This is best done by taking the probability $P_a(t,\varphi)$ at

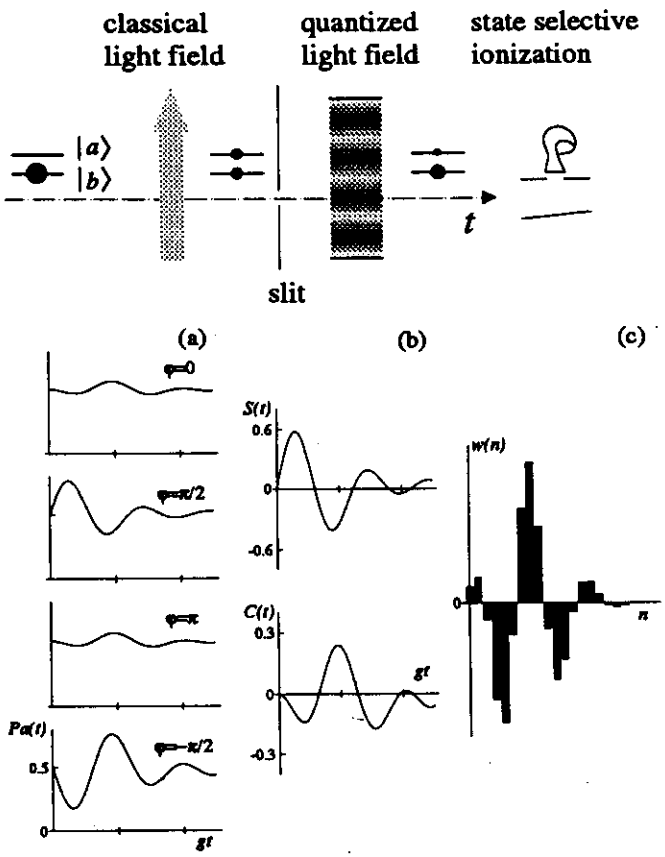

FIG. 1. Quantum state endoscopy. Experimental setup (top): An appropriate classical light field prepares a two level atom in a coherent superposition $\frac{1}{\sqrt{2}}\left(|a\rangle + e^{i\varphi}|b\rangle\right)$. The so-prepared atom interacts with a single mode of the radiation field which is in a pure quantum state described by photon number probability amplitudes w_n. A narrow slit fixes the position where the atom enters the quantized light field and determines the vacuum Rabi frequency g. We probe the internal state of the atom leaving the cavity via state selective field ionization and choose different interaction times by selecting different atomic velocities. We record the atomic population $P_a(t,\varphi)$ in the excited state $|a\rangle$ as a function of time for four different phases φ. Data analysis (bottom): From these four curves (a) we form appropriate linear combinations S and C shown in (b) and extract from them the probability amplitudes w_n of the initial field state (a). For the sake of simplicity we have chosen a Schrödinger cat with real amplitude $\alpha = 2.5$ and phase $\vartheta = 0.9$. Here w_n is real.

four different values of the phase φ. Indeed for the special choice $\varphi = -\frac{\pi}{2}, 0, \frac{\pi}{2}, \pi$ we can define the complex function

$$S(t) \equiv P_a(t,\pi/2) - P_a(t,-\pi/2) + i\left[P_a(t,\pi) - P_a(t,0)\right] = \sum_{n=0}^{\infty} \sin\left(2\Omega_n t\right) w_n w_{n+1}^* \tag{7}$$

only containing the cross terms $w_n w_{n+1}^*$. Similarly we can use the same four measured probabilities to form the real function

$$C(t) \equiv P_a(t,-\pi/2) + P_a(t,0) + P_a(t,\pi/2) + P_a(t,\pi) - 2 = \sum_{n=0}^{\infty} \cos\left(2\Omega_n t\right)\left(|w_n|^2 - |w_{n+1}|^2\right) - |w_0|^2. \tag{8}$$

Now we are left with the mathematical problem to first invert Eqs. (7) and (8), that is to calculate

$$a_n = w_n w_{n+1}^* \tag{9}$$

and

$$b_n = |w_n|^2 - |w_{n+1}|^2 \tag{10}$$

from the measured functions $S(t)$ and $C(t)$ and then to obtain from the nonlinear Eqs. (9) and (10) the complex valued numbers w_n. Indeed by eliminating w_{n+1} or w_n from Eqs. (9) and (10) we find a quadratic equation for $|w_n|^2$ or $|w_{n+1}|^2$, respectively. The corresponding relevant solutions [12] read

$$|w_n|^2 = \frac{1}{2}\left(b_n + \sqrt{b_n^2 + 4|a_n|^2}\right) \tag{11}$$

and $|w_{n+1}|^2 = \frac{1}{2}\left(-b_n + \sqrt{b_n^2 + 4|a_n|^2}\right)$ or equivalently

$$|w_n|^2 = \frac{1}{2}\left(-b_{n-1} + \sqrt{b_{n-1}^2 + 4|a_{n-1}|^2}\right). \tag{12}$$

According to Eqs. (9) and (10) $a_{-1} \equiv 0$ and $b_{-1} \equiv -|w_0|^2$, since $w_{-1} = 0$ following from Eq. (2). Hence we can find the ***absolute values*** of the probability amplitudes w_n from these equations, whereas the ***phases*** we finally obtain by the recurrence relation

$$w_{n+1} = a_n^*/w_n^*, \tag{13}$$

following from Eq. (9). Since the quantum state of the light field is defined up to an overall phase factor, we choose $w_0 = |w_0|$ to be real.

Now we return to the problem of finding the coefficients a_n and b_n. In principle we have to determine an infinite number of probability amplitudes w_n and hence an infinite number of a_n and b_n. However, physical states of the radiation field are normalized and consequently the amplitudes $|w_n|$ have to decay to zero for n much larger than the mean photon number $\bar{n}$. Hence, when we want to find $w_0, w_1, \ldots, w_{n_{max}}$ with $n_{max} \gg \bar{n}$ we have to solve Eqs. (7) and (8) for $n_{max} + 1$ unknown complex valued coefficients. Consequently it is enough to measure the functions $S(t)$ and $C(t)$ for at least $n_{max} + 1$ discrete interaction times t_ν in order to invert [13] the two sets of linear equations

$$S(t_\nu) = \sum_{n=0}^{n_{max}} \sin\left(2\Omega_n t_\nu\right) a_n \tag{14}$$

and

$$C(t_\nu) = \sum_{n=-1}^{n_{max}-1} \cos\left(2\Omega_n t_\nu\right) b_n. \tag{15}$$

In summary we find from the set of measured data $\{S(t_1), C(t_1);\ S(t_2), C(t_2); \ldots\}$ by inversion of the linear equations (14) and (15) the coefficients a_n and b_n which via Eqs. (11) and (12) provide the absolute values of the photon number probability amplitudes w_n. Their phases

follow from the recurrence relation Eq. (13) using the complex valued coefficients a_n.

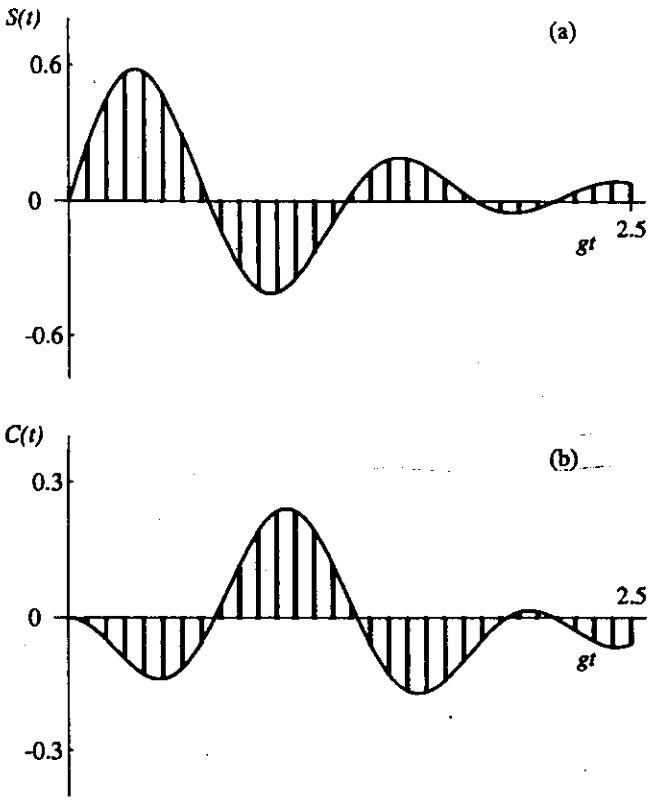

FIG. 2. Measured functions $S(t)$ and $C(t)$ for a Schrödinger cat state, Eq. (16), with amplitude $\alpha = 2.5$ and phase $\vartheta = 0.9$. The solid lines represent the analytic expressions, Eqs. (7) and (8), whereas the bars indicate the corresponding values for 30 discrete interaction times t_ν in units of g^{-1}.

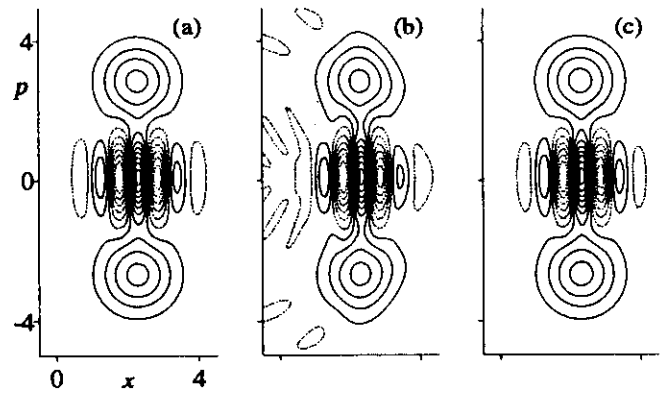

FIG. 3. Reconstruction of a Schrödinger cat via quantum state endoscopy. In (a) we display the field state to be measured by the contour lines of its Wigner function. Solid lines indicate domains of phase space where the Wigner function takes on positive values whereas dashed lines display domains of negative values. In (b) and (c) we show the reconstructed Wigner function for $n_{max} = 18$ and 25, respectively. The latter is an excellent reconstruction of the initial field state (a). We have used the parameters, $gt = 2.5$ and $\Delta v/v = 1.5\%$, of the experiment [7]. For the Schrödinger cat we have chosen the amplitude $\alpha = 2.5$ and the phase $\vartheta = 0.9$.

Now we recognize that the function S alone would have allowed us to get the probability amplitudes w_n: we determine the coefficients a_n by inverting Eq. (14) and find w_{n+1} by iteration using Eq. (13). Nevertheless the function $C(t)$ defined in Eq. (8) is of central importance. Despite the fact that it is free of charge, that is it can be constructed from the already existing data, it provides two independent solutions, Eqs. (11) and (12), for each $|w_n|$. Moreover it is solely due to this function C that we have an explicit expression for $|w_n|$ rather than a recurrence relation. Consequently in the present scheme errors in measured data are not transferred from one amplitude $|w_n|$ to the others.

In order to illustrate this idea of state measurement we reconstruct the Wigner function [14] of a Schrödinger cat state [15]

$$|\Psi_F\rangle = \mathcal{N}\left\{|\alpha e^{i\vartheta}\rangle + |\alpha e^{-i\vartheta}\rangle\right\} \tag{16}$$

with the amplitude $\alpha = 2.5$ and the phase $\vartheta = 0.9$. Here $\mathcal{N}$ is the normalization constant. In Fig. 2 we show the functions S and C calculated for this state via Eqs. (7) and (8) as a function of the interaction time and select for the data analysis 30 discrete interaction times t_ν uniformly distributed over the same region. Here we have chosen a time domain up to $gt = 2.5$, a parameter regime accessible [7–9] by current experiments. With the help of these discrete *measurement data* we reconstruct the quantum state of the light field $|\Psi_F\rangle$. We show the contour lines of the corresponding Wigner function of the Schrödinger cat for two different cut off parameters n_{max} in Fig. 3. Here we have taken into account a velocity distribution [16] of the atoms with a precision $\Delta v/v = 1.5\%$ already available in the experiment of Ref. [7]. We note the excellent agreement between the reconstructed and the initial Wigner function.

We conclude summarizing our main results: We have presented a novel scheme to measure the internal structure of a quantum state of the radiation field in a cavity. The simplicity of the data analysis – a matrix inversion, the solution of a quadratic equation and an iteration – speaks for itself. The state of the art of single atom experiments in the microwave [7,8] and optical [9] domain allows for the experimental realization of quantum state endoscopy.

This work was partially supported by Q.E.D. Associates and the Human Capital and Mobility program. One of us (E.M.) thanks the Deutsche Forschungsgemeinschaft for support.

[1] Endoscopy (*gr.*): *éndon* inside, *skopeîn* to look at
[2] For the theory of quantum state tomography see K. Vogel and H. Risken, Phys. Rev. A **40**, 2847 (1989) and for the experiment see D. T. Smithey, M. Beck, M. G. Raymer, and A. Faridani, Phys. Rev. Lett. **70**, 1244 (1993).

[3] The method of nonlinear atomic homodyne detection proposed by M. Wilkens and P. Meystre, Phys. Rev. A **43**, 3832 (1991) and the technique of probing a quantum state via atomic deflection suggested by M. Freyberger and A. M. Herkommer, Phys. Rev. Lett. **72**, 1952 (1994) allows to measure the state without taking the field out of the resonator.

[4] The intriguing eight port homodyne detector presented in J. W. Noh, A. Fougères, and L. Mandel, Phys. Rev. Lett. **67**, 1426 (1991) and N. G. Walker and J. E. Carroll, Opt. Quant. Electron. **18**, 355 (1986) allows to measure the Q-function of the input field. For the theory, see, e.g., M. Freyberger, K. Vogel, and W. P. Schleich, Phys. Lett. A **176**, 41 (1993) and U. Leonhardt and H. Paul, Phys. Rev. A **47**, R2460 (1993).

[5] The problem of determining the complete wave function from the probability distributions for position and momentum – the so-called phase retrieval problem – was recently investigated by A. Orlowski and H. Paul, Phys. Rev. A **50**, R921 (1994).

[6] Strategies to gain partial information such as the photon statistics about a quantum state are presented, e.g., in M. Fleischhauer and W. P. Schleich, Phys. Rev. A **47**, 4258 (1993); M. J. Holland, D. F. Walls, and P. Zoller, Phys. Rev. Lett. **67**, 1716 (1991); A. M. Herkommer, V. M. Akulin, and W. P. Schleich, Phys. Rev. Lett. **69**, 3298 (1992) and B. M. Garraway, B. Sherman, H. Moya-Cessa, P. L. Knight, G. Kurizki, Phys. Rev. A **49**, 535 (1994).

[7] M. Brune, P. Nussenzveig, F. Schmidt-Kaler, F. Bernardot, A. Maali, J. M. Raimond, and S. Haroche, Phys. Rev. Lett. **72**, 3339 (1994); M. Brune, S. Haroche, V. Lefevre, J. M. Raimond, and N. Zagury, Phys. Rev. Lett. **65**, 976 (1990).

[8] O. Benson, G. Raithel, and H. Walther, Phys. Rev. Lett. **72**, 3506 (1994); G. Rempe, F. Schmidt-Kaler, and H. Walther, Phys. Rev. Lett. **64**, 2783 (1990).

[9] R. J. Thompson, G. Rempe, and H. J. Kimble, Phys. Rev. Lett. **68**, 1132 (1992); G. Rempe, R. J. Thompson, R. J. Brecha, W. D. Lee, and H. J. Kimble, Phys. Rev. Lett. **67**, 1727 (1991).

[10] See, e.g., P. Meystre and M. Sargent III, *Elements of Quantum Optics* (Springer, Berlin, 1991).

[11] In the microwave domain spontaneous emission does not play any role, whereas in the optical domain the interaction times required by the present scheme are short compared to the spontaneous life time. See Ref. [9].

[12] Here we have only taken the sign which guarantees $|w_n|^2 \geq 0$.

[13] For the matrix inversion we use the so-called *Singular Value Decomposition*–method. This allows us to invert quadratic as well as non-quadratic (for the case of an overdetermined set of equations) matrices even when they are almost singular. In this context the so-called χ^2–test can be used as a measure for the quality of the reconstructed state. For a detailed discussion see, e. g., W. H. Press, S. A. Teukolsky, W. T. Vetterling, and B. P. Flannery, *Numerical Recipes* (Cambridge University Press, 1992).

[14] M. Hillery, R. F. O'Connell, M. O. Scully, and E. P. Wigner, Phys. Rep. **106**, 121 (1984).

[15] W. Schleich, M. Pernigo, and Fam Le Kien, Phys. Rev. A **44**, 2172 (1991). M. Brune, S. Haroche, J. M. Raimond, L. Davidovich, and N. Zagury, Phys. Rev. A **45**, 5193 (1992).

[16] A spread in atomic velocity translates itself in a spread of interaction times. For an arbitrary distribution $W(t,\bar{t})$ of interaction times t centered around the average time $\bar{t}$, the time averaged Eq. (7) now reads

$$\bar{S}(\bar{t}) \equiv \int_{-\infty}^{\infty} dt\, W(t,\bar{t})\, S(t)$$
$$= \sum_{n=0}^{\infty} \int_{-\infty}^{\infty} dt\, \sin(2\Omega_n t)\, W(t,\bar{t})\, w_n w_{n+1}^*$$

and analogously for the time averaged $\bar{C}$ from Eq. (8). When we compare this equation to Eq. (7) we note that a spread in the atomic velocity preserves the structure of the equation to be inverted but the function $\sin(2\Omega_n t)$ has been replaced by the corresponding time averaged quantity. Hence the proposed algorithm can deal with an arbitrary distribution $W(t,\bar{t})$ of interaction times. For the reconstruction of the Schrödinger cat we have used a Gaussian distribution

$$W(t,\bar{t}) = \frac{1}{\sqrt{2\pi}\Delta\bar{t}} \exp\left[-\frac{(t-\bar{t})^2}{2(\Delta\bar{t})^2}\right]$$

with $\Delta v/v \cong \Delta\bar{t}/\bar{t}$.

Quantum State Engineering of the Radiation Field

K. Vogel, V. M. Akulin,* and W. P. Schleich†
Abteilung für Quantenphysik, Universität Ulm, D-89069 Ulm, Germany
(Received 25 May 1993)

We give a recipe for how to create an arbitrary field state in a single-mode resonator.

PACS numbers: 42.50.Dv, 32.80.–t

Nonclassical states of light are central to quantum optics. But how can we create them? So far two approaches [1] have been pursued: (i) Find the appropriate Hamiltonian which transforms via unitary time evolution a given initial state to the desired final state. (ii) Make a measurement on one of two entangled quantum systems and obtain the state of the other system by the corresponding state reduction. Mathematically we can always construct the necessary Hamiltonians and entanglements. However, nature limits the possible Hamiltonians and entanglements, and therefore also the variety of states which can be obtained in this way. In the present paper we give a recipe for how to construct *any* desired quantum state of the radiation field using a simple Hamiltonian.

We consider N two-level atoms interacting with a resonant mode of the electromagnetic field in a cavity via the Jaynes-Cummings Hamiltonian. Initially the cavity field is in the vacuum state. We consecutively inject atoms such that there is at most one atom in the cavity at a time. We prepare each atom entering the cavity in a specific superposition of the excited state $|a\rangle$ and the ground state $|b\rangle$. This superposition has to be chosen appropriately [2] in order to drive the state of the cavity field towards the desired state. The measurement of the internal state of the atom after it has passed through the cavity leaves the quantum field in a pure state.

Let us consider one step of this process. Before the injection of the kth atom the cavity field is in a state

$$|\varphi^{(k-1)}\rangle = \sum_n \varphi_n^{(k-1)}|n\rangle\,. \tag{1}$$

The kth atom enters the cavity in the superposition state $|a\rangle + i\varepsilon_k|b\rangle$ controlled by the complex number ε_k [3]. After the interaction, when the atom has left the cavity, the state of the combined atom-field system reads

$$|\Phi^{(k)}\rangle = \sum_n \varphi_n^{(k-1)}\left[C_n^{(k)}|n,a\rangle - iS_n^{(k)}|n+1,b\rangle + i\varepsilon_k C_{n-1}^{(k)}|n,b\rangle + \varepsilon_k S_{n-1}^{(k)}|n-1,a\rangle\right]. \tag{2}$$

Here $C_n^{(k)} = \cos(g\tau_k\sqrt{n+1})$ and $S_n^{(k)} = \sin(g\tau_k\sqrt{n+1})$, where τ_k is the interaction time of the kth atom with the field and g is the atom-field coupling constant.

Now let us make a measurement on the kth atom. If we detect the atom in the excited state our attempt to create the desired field state by our proposed method has failed and we go back to the vacuum state and start the procedure again. However, if we find the kth atom in the ground state we continue the process. In this case the new field state [3] reads

$$|\varphi^{(k)}\rangle = \sum_n \varphi_n^{(k)}|n\rangle\,, \tag{3}$$

where, according to Eq. (2), the new coefficients $\varphi_n^{(k)}$ are given in terms of the old coefficients $\varphi_n^{(k-1)}$ via the recurrence relation

$$\varphi_n^{(k)} = S_{n-1}^{(k)}\varphi_{n-1}^{(k-1)} - \varepsilon_k C_{n-1}^{(k)}\varphi_n^{(k-1)}\,. \tag{4}$$

Each injected atom increases the number of Fock states, building up the cavity field state by one. Therefore, after N atoms have passed through the cavity, the field state, which initially was the vacuum state $|\varphi^{(0)}\rangle$, is a linear combination of $N+1$ number states. But how do we get a desired combination

$$|\psi_d\rangle = \sum_{n=0}^{N} d_n|n\rangle \quad ? \tag{5}$$

For this purpose we have to find that combination

$$|\varphi^{(N-1)}\rangle = \sum_{n=0}^{N-1} \varphi_n^{(N-1)}|n\rangle \tag{6}$$

of N number states which yields $|\psi_d\rangle$ after the Nth atom prepared in an appropriate internal state $|a\rangle + i\varepsilon_N|b\rangle$ has passed through the cavity and has been detected in the ground state. We find the N coefficients $\varphi_n^{(N-1)}$ and the parameter ε_N by solving the set of $N+1$ equations,

$$\begin{aligned} d_N &= S_{N-1}^{(N)}\varphi_{N-1}^{(N-1)} \\ &\vdots \quad \vdots \\ d_n &= S_{n-1}^{(N)}\varphi_{n-1}^{(N-1)} - \varepsilon_N C_{n-1}^{(N)}\varphi_n^{(N-1)} \\ &\vdots \quad \vdots \\ d_0 &= -\varepsilon_N \varphi_0^{(N-1)} \end{aligned} \tag{7}$$

following from Eq. (4). We express the unknown values $\varphi_n^{(N-1)}$ in terms of the known values d_n, starting with the first equation of the set (7), and obtain

$$\varphi_n^{(N-1)} = \sum_{\nu=1}^{N-n}\left[\prod_{\mu=n}^{n+\nu-2}\frac{C_\mu^{(N)}}{S_\mu^{(N)}}\right]\frac{d_{n+\nu}}{S_{n+\nu-1}^{(N)}}\,\varepsilon_N^{\nu-1}\,. \tag{8}$$

0031-9007/93/71(12)/1816(4)$06.00

Substitution of the thus obtained coefficient $\varphi_0^{(N-1)}$ into the last equation of the set (7) yields

$$d_0 + \sum_{\nu=1}^{N} \left[\prod_{\mu=0}^{\nu-2} \frac{C_\mu^{(N)}}{S_\mu^{(N)}} \right] \frac{d_\nu}{S_{\nu-1}^{(N)}} \varepsilon_N^\nu = 0 \tag{9}$$

as the characteristic equation for ε_N.

We solve the characteristic equation numerically and choose one value ε_N from the N roots of Eq. (9). Equation (8) immediately gives us the corresponding coefficients $\varphi_n^{(N-1)}$ of the state $|\varphi^{(N-1)}\rangle$. We take $|\varphi^{(N-1)}\rangle$ as a new desired state which we have to obtain by sending $N-1$ atoms through the cavity. For the state $|\varphi^{(N-1)}\rangle$ we do the same calculations as for the state $|\psi_d\rangle$ and obtain the parameter ε_{N-1} and state $|\varphi^{(N-2)}\rangle$ with $N-1$ coefficients $\varphi_n^{(N-2)}$. We repeat the calculations until we end up with the vacuum state. A string of complex numbers $\varepsilon_1, \varepsilon_2, \ldots, \varepsilon_N$ defines the internal states of a sequence of N atoms we have to inject into the cavity in order to obtain the desired state $|\psi_d\rangle$ from the vacuum state.

We illustrate this method by creating the truncated phase state

$$|\psi_d\rangle = \frac{1}{\sqrt{8}} \sum_{n=0}^{7} |n\rangle . \tag{10}$$

In Table I we give the values $\varepsilon_1, \varepsilon_2, \ldots, \varepsilon_7$ calculated for identical interaction parameters $g\tau_k = \pi/5$. In order to give an impression about the individual steps of the evolution of the field state from the vacuum state to the truncated phase state, Eq. (10), we plot in Fig. 1 the contour lines of the Q function for the field state $|\varphi^{(k)}\rangle$ after the kth atom has passed through the cavity and has been detected in the ground state.

But what is the probability to create the state; that is, what is the probability $\mathcal{P}_N$ to find all atoms in the ground state after they have passed through the cavity? So far we have used unnormalized states for the atoms and the field because it was convenient for calculating ε_k and $\varphi_n^{(k)}$. However, when we need probabilities we have to use normalized field states

$$|\psi^{(k)}\rangle = \sum_{n=0}^{k} \psi_n^{(k)} |n\rangle \tag{11}$$

and atomic field states $(|a\rangle + i\varepsilon_k|b\rangle)/\sqrt{1+|\varepsilon_k|^2}$.

For the coefficients $\psi_n^{(k)}$ we obtain equations similar to Eqs. (7) which read

$$\begin{aligned} \psi_k^{(k)} &= \mathcal{N}_k S_{k-1}^{(k)} \psi_{k-1}^{(k-1)} \\ &\vdots \quad \vdots \\ \psi_n^{(k)} &= \mathcal{N}_k \left[S_{n-1}^{(k)} \psi_{n-1}^{(k-1)} - \varepsilon_k C_{n-1}^{(k)} \psi_n^{(k-1)} \right] \\ &\vdots \quad \vdots \\ \psi_0^{(k)} &= -\mathcal{N}_k \varepsilon_k \psi_0^{(k-1)} . \end{aligned} \tag{12}$$

Here the normalization constant

TABLE I. Internal state $|a\rangle + i|\varepsilon_k| e^{i\beta_k}|b\rangle$ of the kth atom needed to obtain the truncated phase state, Eq. (10), for a fixed interaction parameter $g\tau = \pi/5$. The right column gives the probability $P_b^{(k)}$, Eq. (14), to find the kth atom in state $|b\rangle$ after its interaction with the cavity field provided all earlier atoms have been detected in the state $|b\rangle$. The probability $\mathcal{P}_7$, Eq. (16), to find all atoms in the ground state is $\mathcal{P}_7 = P_b^{(1)} P_b^{(2)} \ldots P_b^{(7)} = 0.01388$.

k	$\lvert\varepsilon_k\rvert$	β_k/π	$P_b^{(k)}$
1	0.5412	−0.5075	0.4938
2	0.5730	0.5102	0.3616
3	0.6951	−0.7585	0.6477
4	0.8283	−0.9977	0.8106
5	1.0562	0.7783	0.7368
6	1.3334	0.5141	0.4918
7	1.5002	−0.5389	0.4086

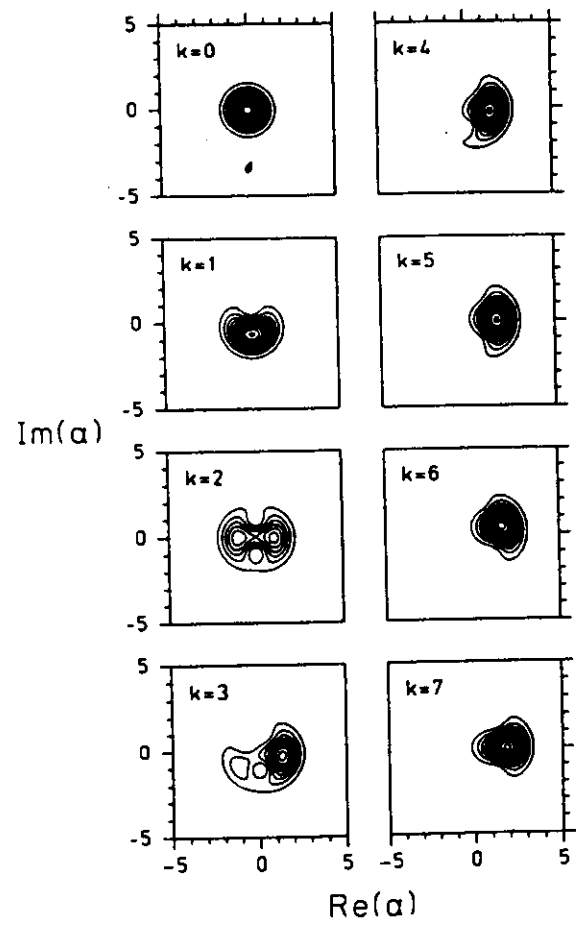

FIG. 1. Contour lines of the Q-function $Q(\alpha) = |\langle\alpha|\varphi^{(k)}\rangle|^2/\pi$ for the field state $|\varphi^{(k)}\rangle$ after the kth atom has interacted with the field and has been detected in the ground state. The parameters for the internal states of the incoming atoms are given in Table I. The contour lines are at $Q = 0.025, 0.050, 0.075, \ldots$.

$$\mathcal{N}_k = \frac{1}{\sqrt{P_b^{(k)}\,(1+|\varepsilon_k|^2)}} \tag{13}$$

consists of two parts: the factor $1/\sqrt{1+|\varepsilon_k|^2}$ which takes into account the normalization of the internal state of the kth atom, and the factor $1/\sqrt{P_b^{(k)}}$ which is due to the normalization of the field state after the state reduction. Here

$$P_b^{(k)} = \frac{\sum_{n=0}^{k} \left| S_{n-1}^{(k)}\,\psi_{n-1}^{(k-1)} - \varepsilon_k\, C_{n-1}^{(k)}\,\psi_n^{(k-1)} \right|^2}{1+|\varepsilon_k|^2} \tag{14}$$

is the probability to find the kth atom in the ground state. From the first equation of (12) follows

$$\psi_N^{(N)} = \prod_{k=1}^{N} \left(\mathcal{N}_k S_{k-1}^{(k)} \right) \psi_0^{(0)} . \tag{15}$$

Since we start from the vacuum state we have $\psi_0^{(0)} = 1$. Moreover, we note that for a normalized desired state we have $\psi_n^{(N)} = d_n$. We substitute $\mathcal{N}_k$ from Eq. (13) into Eq. (15) and obtain for the probability $\mathcal{P}_N$ to find all N atoms in the ground state

$$\mathcal{P}_N = \prod_{k=1}^{N} P_b^{(k)} = \frac{1}{|d_N|^2} \prod_{k=1}^{N} \left[\frac{(S_{k-1}^{(k)})^2}{1+|\varepsilon_k|^2} \right] . \tag{16}$$

The probability $\mathcal{P}_N$ depends on the choice of roots of the characteristic equation, Eq. (9), and the interaction times τ_k. Can we use these "degrees of freedom" to optimize the probability $\mathcal{P}_N$? To get an idea

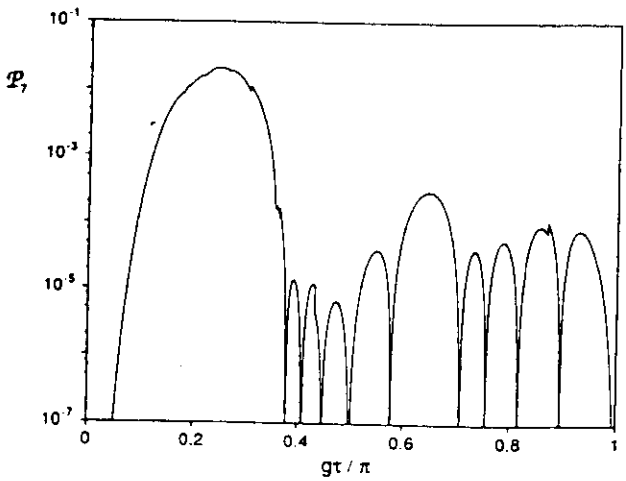

FIG. 2. Probability $\mathcal{P}_7$ to find all seven atoms in the ground state as a function of the interaction parameter $g\tau$ for the truncated phase state, Eq. (10). Here we have chosen ε_k with the smallest absolute value. Note the occurrence of trapping states at $g\tau = \pi/\sqrt{7}$, $g\tau = \pi/\sqrt{6}$, $g\tau = \pi/\sqrt{5}$, $g\tau = \pi/\sqrt{4}$, $g\tau = \pi/\sqrt{3}$, $g\tau = \pi/\sqrt{2}$, $g\tau = 2\pi/\sqrt{7}$, $g\tau = 2\pi/\sqrt{6}$, $g\tau = 2\pi/\sqrt{5}$, and $g\tau = \pi$ where, according to Eq. (16), the probability $\mathcal{P}_7$ vanishes.

TABLE II. Internal state $|a\rangle + i|\varepsilon_k|\,e^{i\beta_k}|b\rangle$ of the kth atom needed to obtain the truncated phase state, Eq. (10). Here we have optimized the interaction parameters $g\tau_k$ as to maximize the probability $\mathcal{P}_7$, Eq. (16), to find all atoms in the ground state. The right column gives the probability $P_b^{(k)}$, Eq. (14), to find the kth atom in state $|b\rangle$ after its interaction with the cavity field provided all earlier atoms have been detected in the state $|b\rangle$. In this case we have $\mathcal{P}_7 = 0.051\,93$.

k	$\lvert\varepsilon_k\rvert$	β_k/π	$g\tau_k/\pi$	$P_b^{(k)}$
1	0.7462	−0.6016	0.5000	1.0000
2	0.8513	0.5569	0.3370	0.5655
3	0.8543	0.7427	0.2780	0.7435
4	0.9972	−0.6821	0.2477	0.6265
5	1.2000	−0.5256	0.2363	0.5196
6	1.3198	0.5097	0.1937	0.4366
7	1.1003	1.0000	0.1524	0.8690

of the possibilities of this optimization let us consider the simplest case of identical interaction times $\tau_k = \tau$ for the example of the truncated phase state, Eq. (10). The dependence of the probability $\mathcal{P}_7$ on the interaction parameter $g\tau$ is shown in Fig. 2. For this curve we have chosen for each atom the ε_k with the smallest absolute value. We note that $\mathcal{P}_7$ increases for increasing interaction parameter $g\tau$ and reaches its maximum $\mathcal{P}_7 \approx 0.020\,67$ at $g\tau \approx 0.2445\pi$ and then decreases. Moreover, trapping states, that is, interaction parameters $g\tau$ with $\sin(g\tau\sqrt{n}) = 0$ $(n = 1, 2, \ldots, 7)$, manifest themselves in vanishing probabilities $\mathcal{P}_7$ as apparent from Eq. (16). As a general rule the maximum value for the probability occurs for interaction parameters smaller than those corresponding to trapping states.

In the next step of the optimization we allow each atom to have its individual interaction time τ_k with the cavity field. In Table II we have chosen τ_k such that the probability $\mathcal{P}_7$ to find all seven atoms in the ground state has a maximum. Using this strategy we increase $\mathcal{P}_7$ up to the value $\mathcal{P}_7 \approx 0.051\,93$.

In conclusion we emphasize that we can construct *any* superposition of the first $N+1$ number states from the vacuum state by injecting N appropriately prepared atoms into a cavity and detecting all of them in the ground state. Furthermore, we note that the Jaynes-Cummings Hamiltonian is not crucial for this method. Similar interactions between field and atom can also be used provided that they allow for energy exchange between field and atoms.

The work of W.P.S. is partially supported by QED Associates.

* Also at Moscow Institute of Physics and Technology, Dolgoprudny, Moscow, Russia.
† Also at Max-Planck-Institut für Quantenoptik, D-85748 Garching, Germany.

[1] For the generation of number states see, for example,

J. Krause, M. O. Scully, and H. Walther, Phys. Rev. A 36, 4547 (1987); J. Krause, M. O. Scully, T. Walther, and H. Walther, Phys. Rev. A **39**, 1915 (1989); P. Meystre, Opt. Lett. **12**, 669 (1987); P. Meystre, in *Squeezed and Nonclassical Light*, edited by P. Tombesi and E. R. Pike (Plenum, New York, 1988); H. Paul, J. Mod. Opt. **38**, 515 (1989); M. Brune, S. Haroche, V. Lefevre, J. M. Raimond, and N. Zagury, Phys. Rev. Lett. **65**, 976 (1990); M. J. Holland, D. F. Walls, and P. Zoller, Phys. Rev. Lett. **67**, 1716 (1991). For the generation of Schrödinger cats see, for example, M. Brune, S. Haroche, J. M. Raimond, L. Davidovich, and N. Zagury, Phys. Rev. A **45**, 5193 (1992); P. Meystre, J. J. Slosser, and M. Wilkens, Opt. Commun. **79**, 300 (1990); for the preparation of a particle in an arbitrary quantum state by "catching" it in an appropriate potential constructed out of the corresponding wave function, see W. E. Lamb, Phys. Today **22**, No. 4, 23 (1969).

[2] We can obtain any superposition of the excited state $|a\rangle$ and the ground state $|b\rangle$ from the state $|a\rangle$ or $|b\rangle$ by applying an appropriate classical field.

[3] In order to keep the mathematics simple we use here unnormalized atomic states and field states.